UNIVERSITAT POLITÈCNICA DE VALÈNCIA

School of Industrial Engineering

Synthesis of Metal Nanoclusters for their Application as
Catalysts in the Electrochemical CO2 Reduction

Master's Thesis

Master's Degree in Industrial Engineering

AUTHOR: Midré , Sabine Eliane

Tutor: García Gómez, Hermenegildo

External cotutor: GOBERNA FERRON, SARA

ACADEMIC YEAR: 2022/2023

INDUSTRIAL ENGINEERING MASTER THESIS

SYNTHESIS OF METAL NANOCLUSTERS FOR THEIR APPLICATION AS CATALYSTS IN THE ELECTROCHEMICAL CO2 REDUCTION

AUTHOR: SABINE ELIANE MIDRE

SUPERVISOR: HERMENEGILDO GARCIA

SARA GOBERNA FERRON

Academic year: 2022-23

1. Introduction

1.1. CO$_2$ Reduction Reaction

The influence of CO$_2$ in the atmosphere on the climate on the surface of the earth has already been known for over a century.(Arrhenius, 1896; Keeling, 1997) But now more than ever it is crucial to reduce greenhouse gases (GHG) like CO$_2$ and to develop environmentally friendly energies and fuels. In 2021 the global average atmospheric Carbon Dioxide was 414.72 parts per million (ppm), which is a new historic high and a high jump in concentration when compared to the years before.(Lindsey, 2022) Already in 2008 The Intergovernmental Panel on Climate Change (IPCC) released an assessment report which stated that if the 2°C target should be achieved, the GHG concentrations would have to be stabilized around 445 to 490 ppm CO$_2$ equivalents. This includes not only CO$_2$ but also other GHGs like Methane and fluorinated gases. When the 2 °C target is observed, a concentration of 400 ppm of only CO$_2$ shouldn't have been surpassed.(EEA, 2008) Seeing that the threshold was already surpassed by over 14 ppm, it is crucial not only to reduce the CO$_2$ emissions, but also to capture the CO$_2$ of the atmosphere. CO$_2$ reduction is a promising approach to tackle this issue by using it and converting it into valuable products.(Pei, 2021; Wang *et al.*, 2021) With the expansion of renewable energies and their fluctuating nature, it is crucial to store the energy when it is produced but not yet needed. The excess energy in the electric power system could be used to power the CO$_2$ reduction and store chemical energy.(Pei, 2021)

The urgency to reduce atmospheric CO$_2$ levels leads to the development of different technologies for CO$_2$ reduction conversion. The methods can be chemical, photochemical, electrochemical and photoelectrochemical. The most promising strategy due to multiple advantages is electro-catalytical CO$_2$ reduction. For example, the reaction conditions are mild, operating at room temperature and at atmospheric pressure, which would greatly benefit large scale applications.(Pei, 2021) Also the electrolytes are recyclable and if the electricity to drive the reaction is made by renewable energies it even is environmentally friendly.(Wang *et al.*, 2021)

There are two major issues regarding the CO$_2$ reduction. Both of them will be addressed in this work. The first is that CO$_2$ is chemically inert due to its double linear bonding. The second is that the CO$_2$ reduction is competing with Hydrogen Evolution Reaction (HER) since both are happening in the same potential range.(Wang *et al.*, 2021)

Half reactions	Electrode potentials, E_0 (V vs SHE, pH = 7)
$2CO_2 + 12H^+ + 12e^- \rightarrow$	-0.33
$2CO_2 + 12H^+ + 12e^- \rightarrow C_2H_4 + 4H_2O$	-0.35
$2CO_2 + 6H^+ + 6e^- \rightarrow CH_3OH + H_2O$	-0.38
$2H^+ + 2e^- \rightarrow H_2$	-0.42
$CO_2 + 4H^+ + 4e^- \rightarrow HCHO + H_2O$	-0.51
$CO_2 + 2H^+ + 2e^- \rightarrow CO + H_2O$	-0.53
$CO_2 + 2H^+ + 2e^- \rightarrow HCOOH$	-0.61
$CO_2 + e^- \rightarrow CO_2^{\cdot-}$	-1.90

Table 1 Half reactions and their corresponding electrode potentials for CO_2 reduction and the competing HER

In this work the gaseous and liquid products have been analyzed. Since the CO_2 reduction is a multielectron transfer reaction, the energy barrier for each electron transfer must be overcome. The overpotential is determined by the step which costs the most energy during the reaction mechanism. Subsequently, the CO_2 reduction will commence at the given potential in Table 1 but will only show significant CO production at lower potentials.

1.2.   Gold Clusters as Catalysts

Investigation of Nanoclusters for heterogeneous catalysis is emerging due to their well-defined composition, high tunability and large surface to volume ratio (Zhao *et al.*, 2018). Nanoclusters have a metal core smaller than about 2nm, whereas Nanoparticles have a metal core larger than about 3nm. The differentiation is obtained by the drastically different optical properties of Nanoparticles and Nanoclusters, due to the Quantum Size Effect. At the scale of the size of Nanoclusters only a few metal cores with specific sizes and number of atoms per core are stable over long periods of time. These Nanoclusters possess a high stability and similar physical properties. These specific sizes are stable due to their physical packaging and a stabilizing outer electronic shell. Nanoparticles obtain due to these special properties discrete and molecular-like energy-levels that may account for their good electric properties.(Yau, Varnavski and Goodson, 2013) These metal Clusters behave like molecules and larger ones exhibit a nonmetal-to-metallic transition. Gold Nanoclusters (AuNCs) are the most studied among the Metal-Nanoclusters due to a more mature synthesis and stability.(Wu and Jin, 2021)

In this work only Nanoclusters with exact 25 Gold atoms were used. The Gold cores are protected by thiolate ligands to create a higher stability. The exact structure of these Nanoclusters is $Au_{25}(SC_2H_4Ph)_{18}$, which called in short $Au_{25}SR$. The SR refers to thiolate ligands protecting the metal core. The structure of the Cluster has an icosahedral Au_{13} core surrounded by six dimeric Au_2S_3 structures (Figure 1). The synthesis of $Au_{25}SR$ consists out of two steps: Reduction of Au(III) to Au(I) with SR complexes and then reducing Au(I) to Au(0) with $NaBH_4$. This procedure with harsh conditions only allows Nanoclusters with a stable number of elements to be formed.
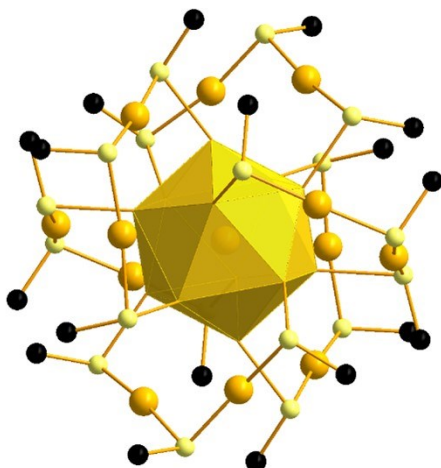
Figure 1 Structure of Au$_{25}$SR Cluster, redrawn from reference (Zhu et al.*, 2008); Yellow: Au, Light yellow: S, Black: C (carbon tales omitted for clarity)*

Kauffman et al. was the first one to observe a spontaneous coupling between Au$_{25}$SR and CO$_2$, which motivated them to investigate Au$_{25}$ for the electrochemical reduction of CO$_2$. The investigations showed, that with the help of Au$_{25}$ a significantly lower overpotential should be reached than with larger Nanoparticles or with bulk Gold. This is due to a unique reactive site of Au$_{25}$ which facilitates C-O double bond activation and H$_{ads}$ formation. It was also found that the exposure of the active sites is crucial to influence the breakage of the CO$_2$ double linear bonding, therefore it is necessary to remove the ligands that protect the Au$_{25}$.(Cai *et al.*, 2022)

1.3. Graphene Species as Support

The support of catalyst plays a huge effect on the catalyst's performance during the investigated reaction. It can influence the selectivity, disperse the catalytic active material, and serves as conduction material for the charges.

The dispersion of the Nanoclusters is crucial for their performance. For a high conversion rate, the concentration of reactants must be high as possible while the products have to be transported away from the active sites. An open structure and spatial far distribution of the active sites improves the flow to and from the active sites. In addition, the dispersion and immobilization of the Nanoclusters is crucial to avoid agglomeration and detachment.

In the past when Graphene was used as support, it was most often used for smaller Particles than the Nanoclusters we used in this work or even single atom-catalysts. A widely researched field are the Metal-Nitrogen-Carbon catalysts which were embedded in all types of graphitic support, such as also in Graphene. These catalysts are immobilized within the Graphene with π- π stacking of the π - conjugation (Wang *et al.*, 2019) or the metal catalysts are directly pyrolyzed with the Graphene-Precursor to have the single atoms directly embedded in the Graphene structure.(Zhang *et al.*, 2019)

1.4. Gold Clusters on Graphene as Catalysts

Rogers et al. already investigated CO_2 reduction with Gold Nanoparticles (AuNP) embedded in functional Graphene Nanoribbons (GNR). They analyzed Graphitic support materials due to their electronic structure leading to strong d-π interactions leading to enhanced dispersion and stabilization of metal Nanoparticles. GNR especially were investigated due to their structural precision and tunability. GNR showed a high microporosity. This facilitated mass transport and a higher active surface area compared to a reference composite prepared from AuNP on Carbon Black (CB). In addition, a higher selectivity towards CO_2 reduction to CO was obtained compared to the AuNP on CB reference. Since the NP on GNR had an effective immobilization a relatively high stability was obtained. In comparison the main deactivation of AuNP on CB was assumed to be aggregation of smaller Particles to bigger ones decreasing the active surface area. This led to significantly lower active surface area after stability tests were done and therefore a low stability was attested.(Rogers *et al.*, 2017)

1.5. Objectives of this work

To reduce the concentration of GHGs in the atmosphere it is crucial to capture and utilize CO_2. An important precursor to produce synthetic fuel is obtained if CO_2 is reduced to CO. With technologies utilizing CO_2 and producing synthetic fuels, two important problems of the current times would be solved. To be able to engineer such technologies applications must be developed. To have environmentally friendly and energy efficient technologies, catalysts with good performance must be developed. Gold Nanoclusters have already been found to be great catalysts to reduce CO_2, now the support of them must be researched to be able to develop suitable catalysts and the corresponding electrodes.

The focus of interest in research is the interaction between active material and support to develop their full potential for catalytic electrochemical CO_2 reduction. Therefore improving the catalyst stability by heterodoping of Graphene materials and improving their performance due to synergistic effects between Nanoclusters and support-material. Additionally, the aim is to recognize the role of each component within the catalytic reaction and engineer their properties to develop a new optimal catalyst for CO_2 conversion.

2. Experimental Part

2.1. Preparation

2.1.1. Preparation of the Graphene and doped Graphenes

The precursor to obtain pure Graphene (G) was Alginic Acid from brown algae. To obtain S-doped Graphene (GS) the precursor was λ-carrageeans (Dhakshinamoorthy *et al.*, 2015) and for N-doped Graphene (GN) it was chitosan (Primo *et al.*, 2012; Candu *et al.*, 2019). All chemicals are by the brand Sigma Aldrich. Around 120 mg of all three precursors were pyrolyzed under Argon flow at 900 °C for 1 hour in a Carbolite Gero Oven. The resulting black powder was then sonicated at 750 W for 1 hour with a Vibra Cell by Sonics with a tip only meant for organic materials to obtain thin sheets of Graphene. The sonicated solution was then dried overnight while being stirred.

2.1.2. Preparation of Gold impregnated Graphene Catalysts

Au$_{25}$ Clusters were synthetized following a literature method (Wu and Jin, 2021) by one of our group members during a short stay at the Institute of Materials Chemistry (Technische Universität Wien, Austria) in the context of a collaboration with Dr. Noelia Barrabés. Therefore, the amount of Au$_{25}$ Clusters available in our lab was limited. Three vials containing 6 mg of Au$_{25}$ each were dissolved in 2 mL of Toluene. To obtain 10 wt% of Gold, 56 mg of the respective Graphenes were added to each vial. For the impregnation to happen, the solutions were stirred and let dry in air over night. The same procedure was applied to obtained Au$_{25}$ supported on Carbon Black (AuCB). A schematic representation of the catalysts preparation is shown in Figure 2 using the preparation of AuG as example.
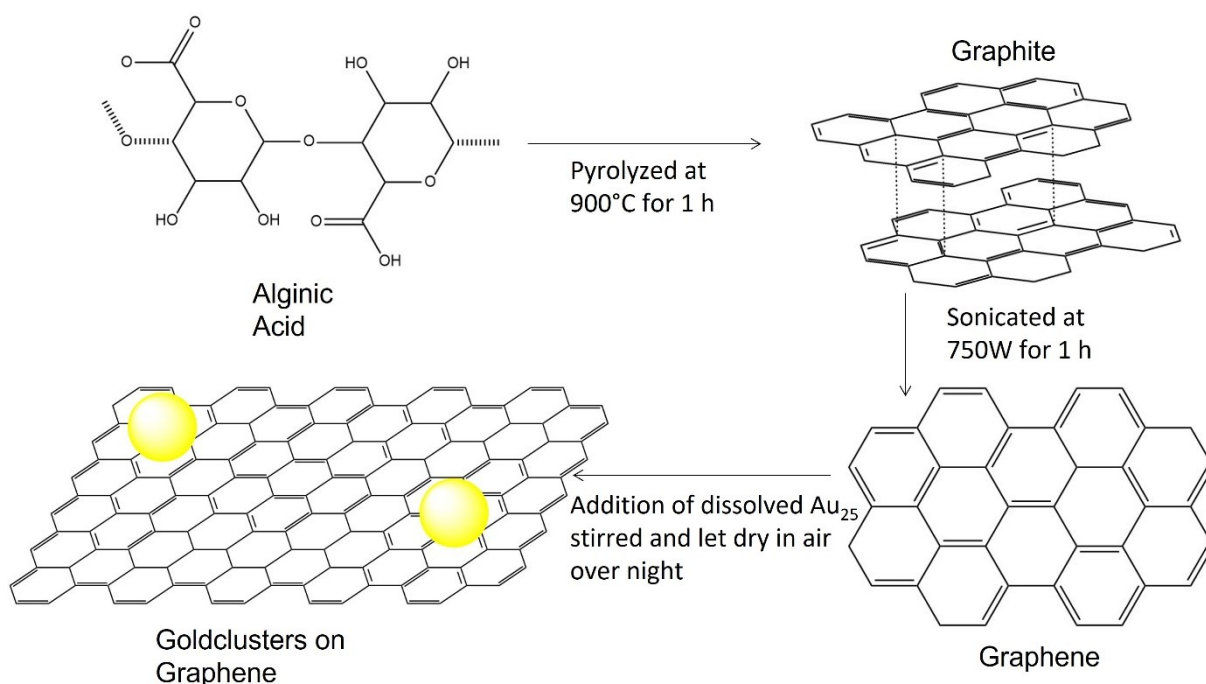

Figure 2 Schematic representation of the preparation process of AuG

2.1.3. Preparation of the Electrodes

The electrode of choice for the Working Electrode (WE) was a Carbon Paper (CP) electrode because of its high surface area, electrochemical activity, electronic conductivity, porosity, ease of handling, and good mechanical strength. The weight of the CP pieces was measured before and after the preparation to be able to tell how much catalyst is deposited on them. To deposit the catalyst on CP a catalyst ink was made. 5 mg of the catalyst powder was measured and mixed with 1 ml Isopropanol. The suspension was then put in a sonicator bath of Branson 5800 for 0.5 to 1 hour. 40 µl of Nafion were added and the mixture was again sonicated in the bath for 5 to 10 minutes. 60 µl of the catalyst ink were slowly deposited using a micropipette on each of the CP electrodes and dried overnight. The amount of catalyst loading was between 0.3 mg and 1 mg.

2.2. Characterization techniques

2.2.1. Raman Spectroscopy

Raman Spectroscopy analyzes the unique electronic states of molecules, which also helps to identify the samples. In Raman Spectroscopy a change of energy and scattering of photons is observed when the sample is irradiated with monochromatic light. There are several possibilities what could happen to a photon when it hits the analyzed molecule: If the outcoming scattered photon has a lower frequency than the light source it is known as Stokes Raman scattering and if the outcoming photon has a higher frequency it is called Anti-Stokes Raman scattering. In both cases the energy change is connected to the unique vibrational modes of the electrons in the molecule.

When irradiated with light, the electron absorbs the photon and gets excited to a higher virtual state. While the electron falls back to a lower vibrational state another photon is emitted. The energy of the initial and emitted photon is different since the initial vibrational state and the one in the end aren't the same. Since these vibrational modes and the possible state transitions are unique to each molecule, the measured spectra of energy shifts can be used as a fingerprint to identify the structure and molecules in the irradiated sample.(McCreery, 2005; Rostron, Gaber and Gaber, 2016)

Between 2 and 3 mg of the catalyst's samples were taken and given to the technicians to analyze the sample. The Raman spectra were recorded on a Renishaw In Via "Reflex" spectrometer connected to a CCD detection system using 514.5 nm excitation laser light provided by a cobalt solid state laser. The laser power on the sample was 15 mW and a total of 10 acquisitions were taken.

2.2.2. XPS Spectroscopy

X-Ray Photoelectron Spectroscopy (XPS) reveals chemical state information of the molecules in a sample. All elements can be detected except Hydrogen and Helium. It uses the photoelectric effect to determine the binding energy in a molecule.

The molecule is irradiated with X-Rays which causes a core electron to be emitted. The kinetic energy is then measured and used to determine the binding energy of the electron with the help of the following equation. It shows that the energy of the X-Ray (hv) is equal to the binding energy (BE) the kinetic energy of the emitted electron (KE) and the work function of the spectrometer (ϕ_{spec}).

$$hv = BE + KE + \phi_{spec}$$

Each element and each combination of covalent bonding has its own specific binding energy, so that the electronic structure can be revealed.(Stevie and Donley, 2020)

To take the XPS measurements between 2-3 mg of each sample were given to the technician to test. XPS spectra were recorded through a SPECS spectrometer equipped with a Phoibos 150 MCD-9 detector. The nonmonochromatic X-Ray source composed of Al and Mg was operated at 200W. Before

data acquisition, the samples were evacuated at 10-9 mba in the spectrometer antechamber. The work function of the device was calibrated with Ag, Au and Cu resulting in a value 4.2440 eV. The measured intensity ratios of the components were obtained from the area of the corresponding peaks after nonlinear Shirley-type background subtraction and corrected by the transition function of the spectrometer.

2.2.3.   Electron microscopy

For the analysis of the size, dispersity, shape, and structure of the catalysts two imaging techniques were used: Transmission Electron Microscopy (TEM) and Scanning Transmission Electron Microscopy (STEM).

For a TEM image, a beam of electrons is transmitted through the sample which then interacts with the sample. Only the electrons which pass by to a detector on the other side of the sample are registered, taking a picture of the penetrability of the sample by electrons.

A TEM picture can be used in many possible ways. For example, the morphology is revealed or the crystal structure of the Graphenes. Also, the Gold Particles can be seen within the catalysts and the size distribution of the Clusters can be calculated.

The STEM is a type of TEM. The difference is that in STEM the electron beam is focused on a fine spot. A whole picture can then be obtained by moving the beam in a raster to methodically scan the sample. With the help of STEM it is also possible to do spectroscopic mapping.

Since the beam must partially shine through the sample it must be thinner than 100 nm thick. That is the reason why the TEM samples needed a special preparation. A small amount of sample was taken (1-2 mg) and dissolved in 1 ml of Ethanol. The suspension was then sonicated in the waterbath for 40-60 min. Afterwards the suspension was left to rest, for the big parts of the Graphene to set at the bottom of the vial. One drop of the top of the suspension was then taken with a capillary and dropped on a TEM sample support mesh grid made of copper. TEM images were recorded via a JEOL JEM 2100F microscope operating under an accelerating voltage of 200 kV.

2.2.4.   NMR

Nuclear Magnetic Resonance Spectroscopy is an analytical technique to obtain knowledge about structures and the bonding of molecules. In this work it is used to analyze the liquid products of the reaction.

As the name already describes, this technique uses the possibility to resonate with the spin of the nuclei of atoms. Compared to other spectroscopic methods the NMR spectroscopy uses the lowest irradiation energy to excite the atom.(Bharti and Roy, 2012) The quantum state of a proton can be excited when a magnetic field is applied. Since the energy levels between the excited state and the relaxed state are so low, an induced emission is necessary to detect the excitation and relaxation. This happens by inducing an electromagnetic alternating field causing the spin of the nuclei to resonate

and to influence all neighboring nuclei. The alternating field is tested at different frequencies to detect the frequency at which the nuclei of the molecules resonate. This frequency is proportional to the magnetic field B_0 which is modified by the chemical surroundings of the atoms in the different positions in a molecule. This modified magnetic field is called B_{eff} and is mainly influenced by the electrons surrounding the nuclei. At higher electronic densities, B_{eff} is weaker, the difference between excited and relaxed state is lower and the resonance frequency is lower. That means when looking at an NMR spectrum a signal will appear upfield/ on the right side. The opposite effect is seen when a molecule has a lower electronic density. The electron density and therefore the ability of the nuclei to resonate also depends on the anisotropy and the steric effects of the electronic structure of the molecules. For example, electrons in double or triple bonds show a bigger downshift.

Alcohol and Amine protons cause often a more complicated spectrum since they have a fast chemical exchange with neighboring atoms. By adding D_2O the corresponding protons are substituted by Deuterium and a simplified spectrum is obtained.(Diehl, 2008)

The signal intensity in the NMR spectrum is proportional for the number of nuclei in the sample that cause the resonance. This leads to the possibility to compare the ratio of two signals obtained in the spectrum and if the molar amount of one of the compounds is known then the other one can be calculated. In our case DMSO was added to reference the amount of Formic Acid that was obtained.

To prepare the samples for the NMR measurement 0.5 ml of the used electrolyte were taken and filled in an NMR Tube together with 100 µl of DMSO and 20 µl of D_2O. Since the electrolyte was taken after several CAs at different potentials but with the same electrode, only a quantitative result can be obtained and not a qualitative result with which the Faradaic Efficiency (FE) of the material at a specific potential. The samples were tested for their 1H protons with a Bruker 400 MHZ Avance Neo.

2.2.5.   UV-Vis Spectroscopy

UV-Vis is an analytical method to identify optical and electronic properties of materials. In spectrophotometry a sample is irradiated with light and the light that passes through the sample and is not absorbed is analyzed. The absorbance spectrum of each material is different and therefore can be used like a fingerprint. As previously mentioned in 1.2 Nanoclusters have special optical properties, which separates them from Nanoparticles and which allow us to observe changes in structure.

Samples for UV-Vis spectrophotometry are most often liquids. Therefore, the support had to be separated from the Gold Clusters prior to the analysis. To do so, all samples were mixed with Toluene to dissolve the Gold Clusters and filtrated through a filter with a pore size of 0.22 µm to eliminate the Graphene. Then, the liquid was placed in a transparent cuvette for measurements. The spectra were acquired via a Varian Cary 5000 spectrophotometer in the range 300-900 nm.

2.2.6.   XRD

The crystalline structure of materials can be analyzed with X-Ray-Diffraction. Amorphous materials like glass do not produce a significant signal and can therefore not be analyzed with XRD.

Since the wavelength of X-Rays is similar to the spacing in between atoms in a crystal, diffraction can be used to determine the structure of the crystal. An X-Ray is an electromagnetic wave, that when striking a crystalline structure is scattered symmetrically. Since the beam passes through some layers of the crystal and is radiated on an angle on the sample an optical path difference occurs. Depending on the angle of the irradiation constructive or destructive interference between the scattered rays can happen.

Powder XRD holds some advantages in comparison to traditional XRD. Samples are easier to prepare and multicrystalline materials can easily be analyzed. The powder must be powders on flat surfaces made coplanar to the sample holder. With powder XRD materials can be differentiated into crystalline, semi-crystalline and amorphous materials.(Niu *et al.*, 2020)

Since the XRD measurements were taken at the end of all characterization measurements only a small amount of Catalyst material was left. Therefore, mirrored XRD holders were used. Around 0.5 mg of each of the three Gold on Graphene catalysts were taken and dissolved in 1 ml of Acetone and sonicated in the bath sonicator for about 0.5 hours. Then the solution was drop casted drop by drop on the mirrored holder, till all the sample was on the holder. The sample dried in between each new drop. PXRD diffraction patterns were acquired through a Shimadzu XRD-7000 diffractometer employing a Cu-k-α irradiation source (λ=1.5418 Å) operational at 40kw and 40 mA. All data acquisition was done with a scanning speed of 10°/min in the 2-90 range (2θ°).

2.2.7.   Gas Chromatography

Gas Chromatography (GC) is used to identify and quantify the molecules in the analyzed sample. In GC the sample is injected into a stream of a carrier gas also called mobile phase. It is then streamed through a long tube called column with a viscous coating called stationary phase. In this column the samples components are separated based on their ability to mix with the mobile and stationary phase. The reason for the gases to mix better with the stationary phase can be different, for example their boiling point or the size of the gas molecules. Their ability to mix with the stationary phase influences the retention time of the gas in the column, so that different gases are detected at the end of the chromatograph at different instants of time. With the knowledge of the retention time of specific gases a qualitative analysis of components can be made. When in addition the intensity of the signal at the detector is calibrated, it is also possible to obtain information about the amount of the different components of the gas.(Harvey, 2000)

For the analysis of H_2 as a product a volume of 1.5 mL was taken from the gas phase of the reactor. The first 0.5 mL were injected into the line of the corresponding GC, leading to the saturation of the line with the product gases. Afterwards the rest of the volume was injected to obtain the amount of product in 1 mL of gas. Before and after each of these procedures the line leading towards the GC was

purged with Argon gas. Analysis of the evolved gases has been carried out through a micro-GC with two columns (Molsieve 5A and PorePlot Q) and a TC detector.

To analyze the amount of CO in the sample a volume of 100 µL were taken from the gas phase in the reactor and injected directly into the corresponding GC. The evolved gases were analyzed using a gas chromatograph (Agilent 7890A) equipped with Carboxene 1010 column analyzing CO_2, CO and up to C4 hydrocarbons.

Quantification of the percentage of each gas was based on prior calibration of the system injecting mixtures with known percentage of gases with following equation.

$$\mu moles = \frac{x * Pressure * Volume\ in\ Reactor * 10^6}{CC * R * Temperature}$$

With the help of this equation, we get the amount of the gases in the whole reactor. We need the Calibration Constant (CC) and the amount of the analyzed gas within the taken sample (x).

2.3. Electrochemical Reactions

2.3.1. H-Cell Setup

A glass H-Cell was used to do all the electrochemical reactions. It is named like the letter H because of its similarity to it. It consists of two compartments which are divided by a Nafion membrane. A three-electrode-setup was used to properly separate the investigated reduction reaction and the counter oxidation. An image of the setup can be seen in Figure 3.

The working electrode is the electrode for which the electrochemical half-reaction is investigated. In the same compartment, near to the working electrode is the reference electrode (RE) situated. It is connected via a high-ohmic resistance to the cell, therefore there is no current flow through the reference electrode, and it doesn't take part in any reaction. In electrochemical measurements, Ag/AgCl is usually used as the RE to evaluate the performance of the catalysts in the system. The conversion of Ag/AgCl (saturated KCl) reference electrode to the Reversible Hydrogen Electrode (RHE) is expressed as the following equation (Niu *et al.*, 2020):

$$E_{RHE} = E_{Ag/AgCl} + 0.059 \times pH + E^0_{Ag/AgCl}$$
$$E^0_{Ag/AgCl} = 0.1976\ V\ at\ 25°C$$

In the other compartment of the H-Cell is the counter electrode (CE) located. The current is measured between it and the WE. It also provides the charge compensation for the reaction at the WE. The material of the CE is Platinum. The used H-Cell was filled in each compartment with 20 mL of electrolyte.

The electrolyte used in both compartments is 0.1 M $KHCO_3$ (pH = 7 when the electrolyte was saturated with CO_2). For the electrochemical measurements two types of potentiostats were used. For the Cyclic Voltammetries (see section 2.3.2) and Chronoamperometries a VersaStat3 potentiostation by Ametek was used. For the Electrochemical Impedance Spectroscopy an Interface 5000 by Gamry Instrument was used.

Figure 3 H-Cell Setup with WE, CE and RE

2.3.2. Cyclic Voltammetry

Cyclic Voltammetry (CV) is a popular electrochemical technique to investigate the behavior of a material during reduction and oxidation processes. In a CV a current is measured while the potential is constantly changed. While the potential is scanned towards a more negative potential it is called cathodic sweep and the reduction reactions are benefited. After the lowest potential is reached, the potential starts to rise again, which is called the anodic sweep and giving the possibility of oxidation reactions.

To activate the catalysts, CVs before the actual measurements was done. This procedure made sure, that the previously dry catalysts were fully penetrated by the electrolyte and that the gas diffusion layer on the electrode could be built up at each pore of the catalyst, so that every active site was reachable for every reactant.

Apart of being useful for the activation of catalysts a lot of information can be obtained by doing CVs. To show the general ability of the catalysts to reduce CO_2 a two-part CV was made. At first the cell was purged with Argon, an inert gas, and afterwards multiple CVs were done. Then in the second part of this experiment the cell was purged with CO_2 and again CVs were collected. If the CO_2 takes part in a reaction, a change in the current density can be seen.

To test the decay of an electrode after several hours and different potentials another CV experiment can be performed. This is not an absolute measurement; it is only a relative measurement to compare different electrode decays qualitatively.

2.3.3. Chronoamperometry

A Chronoamperometry (CA) is an electrochemical technique in which a constant potential on a WE is applied and the current response is monitored as a function of time. There are many ways to do CAs, for example pulsed or stepped signals which allow to analyze different aspects of the catalyst's performance. In this case we applied a constant potential over 30 min to be able to analyze the catalytic reaction products. Six different potentials were tested: -0.5 V, -0.6 V, -0.7 V, -0.8V, -0.9V and -1V against RHE.

The purpose of the CAs is to analyze the amount of product gases to find out the activity and selectivity of the different catalyst materials. To have comparable values of the catalysts the Faradaic Efficiencies were calculated with following equation:

$$FE = \frac{n * z * F}{Q} * 100\%$$

The FE is calculated with Q which is the total charge transfer which was obtained during the 30 min reaction of the CAs, the amount of obtained product n and z is the number of transferred elemental charge during the reaction.

2.3.4. Electrochemical Impedance Spectroscopy

The Electrochemical Impedance Spectroscopy (EIS) is used to understand resistances and interface resistances throughout a chemical cell. Each element of an electrochemical cell can be described as an electrochemical resistance within an electric circuit. The resistance between the two clams is defined, by the electrode, the catalyst, the Hemholtz double layer and the electrolyte and its ion transport ability. The Hemholtz double layer can be compared to an electric capacitor, whereas the electrolyte is a regular electrical resistance. To this electrochemical circuit is an AC Voltage applied with a changing frequency. The current is then analyzed since it depends on the frequency. With the help of the current, the imaginary resistance due to the capacitance of the Hemholtz layer and real resistance due to the diffusion in the electrolyte can be obtained.

3. Results and Discussion

3.1. Catalysts preparation and characterization

3.1.1. Structural and electronic characterization

The six samples (G, AuG, GS, AuGS, GN and AuGN) were tested with Raman Spectroscopy to evidence the different types of Graphene, their qualities and if some changes within the Graphene happened while being impregnated with the Gold Nanoclusters.

In this work a variety of Graphenes were used, which have intensely been studied by our research group in the past, making it easy to compare the obtained Graphene species to the ones analyzed in literature. The focus of interest while analyzing Graphenes are the D-,G- and 2D Band states. A shift in the Raman spectra at 1590 cm^{-1} is specific for Graphene and the corresponding G-Band and as you can see in Figure 4 (left) is also given in the produced G. Another peak specific for Graphene and Nitrogen structures is at 1360 cm^{-1} which is also seen in Figure 4 at 1350 cm^{-1}.(Candu *et al.*, 2019) The presence of this peak may indicate that the Graphene does not have a good quality. It might have defects or is doped with Nitrogen, which is obviously the case for GN. The broad band with a peak at 2900 cm^{-1} witnesses the 2D band and therefore high quality Graphene sheets.(Primo *et al.*, 2012) The positions of the peaks aren't affected by doping nor by impregnation of the Au_{25} Cluster as it can be seen Figure 4 and in Figure 30 in the Appendix. That leads to the conclusion, that neither doping nor the impregnation of the Graphenes with Au_{25} Cluster changed considerably the electronic structure of the produced Graphenes.
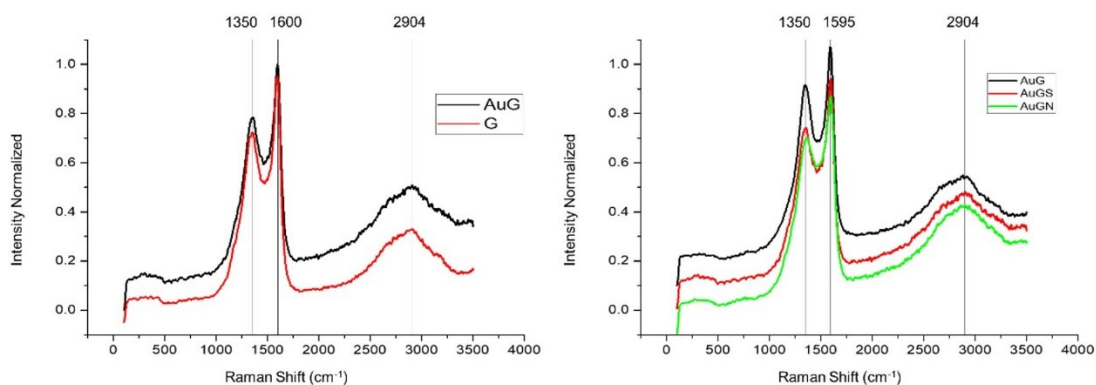

Figure 4 Raman Spectrum of G, AuG (left) and of AuG, AuGS and AuGN (right)

3.1.2. Morphology and composition characterizations

TEM Data

Due to the high importance of the geometrical structure of the Clusters and the support of the Clusters for the performance of the catalyst a thorough study of its physical properties had to be made. To

analyze the morphology of the different Graphene species and the distribution of the Gold Clusters on the support, images with TEM were taken. Since the images reveal the exact structure of the material it is the best characterization technique to study the catalysts morphology.

Figure 5 shows the images taken by TEM of the different Graphene species. The images of larger scale (b, d, f) show that all three samples have the characteristic sheet structure of Graphene.

The undoped Graphene shows a high level of order in small scales around a few nm as well as in larger scales around 50 nm. A crystalline structure can be seen in (a) which evidences high quality Graphene.

The Sulfur doped Graphene shows the highest degree of disorder among the three analyzed Graphene species. There is no characteristic crystalline structure evident in the small-scale image like in G. In Figure 5 d can be seen, that the different Graphene sheets are more amorph, meaning they are smaller and have a more irregular shape.

The Nitrogen doped Graphene (Figure 5 e,f) is amorph, but still shows a crystalline structure like G. On a larger scale it is obvious that the sheets have a more irregular shape than of undoped Graphene, but it is still more ordered than the GS.
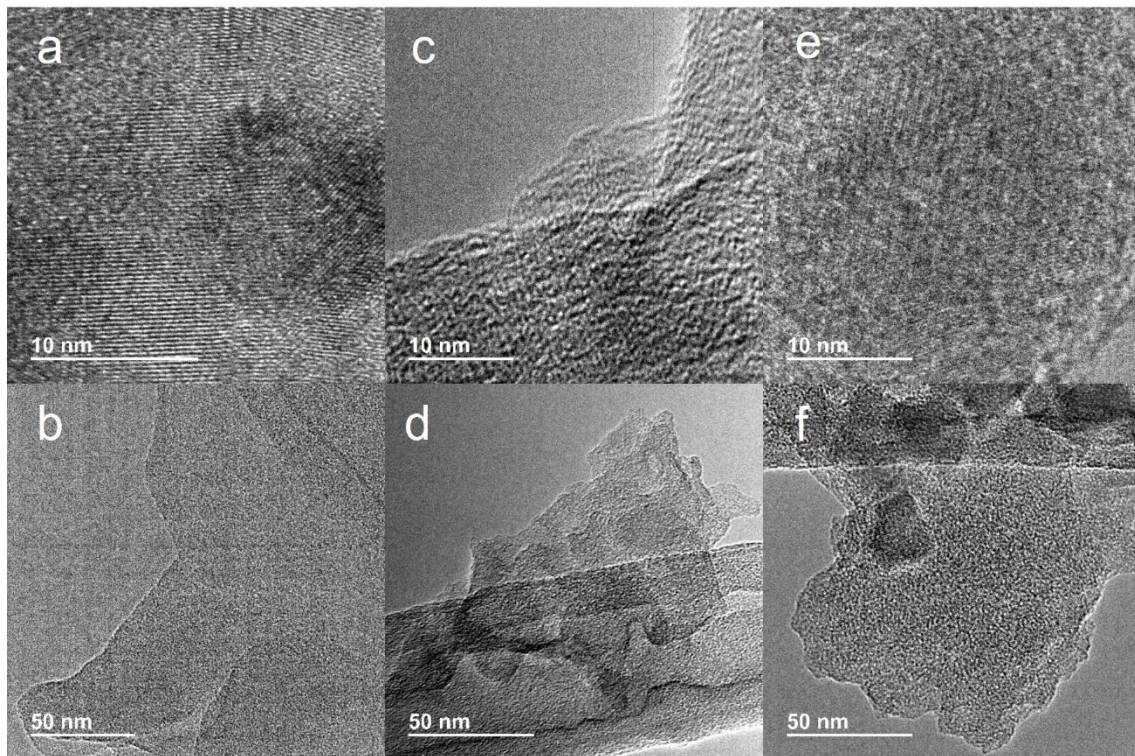
Figure 5 TEM Images of G, GS and GN (from left to right)

Figure 6 shows TEM images of the three different Graphene species impregnated with the Gold Clusters. In none of them is the crystalline structure of Graphene evident but the crystalline structure of the Gold Particles can be seen.

The Gold Particles are well distributed among the support, especially in the Graphene species with a higher degree of order. The spatial distribution of the Gold Clusters can also be seen in the STEM pictures of the catalysts (Figure 7) in which the Graphene support can only be seen in a dark grey, while the Gold Particles are seen in an obvious white. The Gold Clusters on G are well distributed and show a high degree of order. Whereas the STEM pictures of AuGS show that it is very amorph.

The STEM picture taken from AuGN shows a good distribution of Nanoclusters but as well some degree of three-dimensionality, also causing the material to be more amorph.
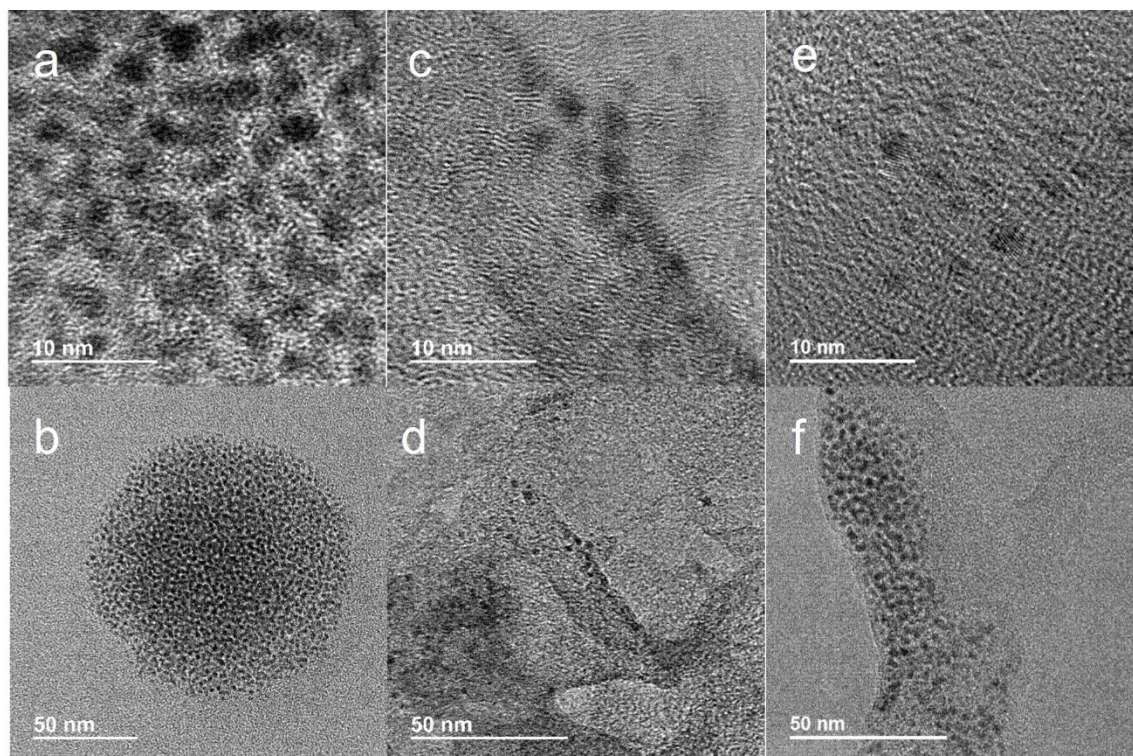
Figure 6 TEM Images of AuG, AuGS and AuGN (from left to right)
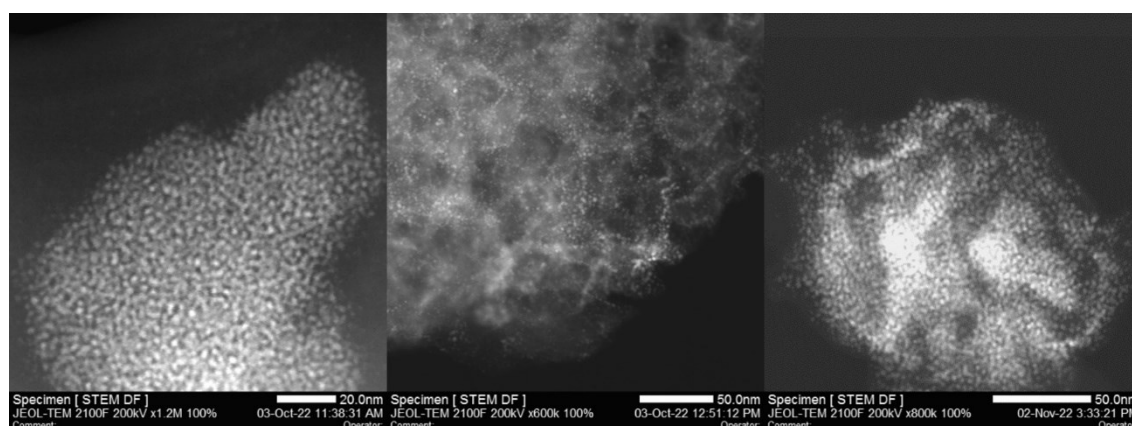
Figure 7 STEM Images of AuG, AuGS and AuGN (from left to right)

An elemental mapping with STEM was made to localize the distribution of the different elements within the catalysts.

Figure 8 shows the STEM picture and the corresponding mapping of AuG. It is evident that the Gold is homogeneously distributed on the Graphene support. The Gold Clusters are also only on the support and not loose on the sample. As expected, Oxygen was detected by STEM since the environment of the sample was air. For the following STEM images the Oxygen was ignored, since the Oxygen of the atmosphere doesn't play a role in the catalyst performance and therefore is not important for the analysis. As Figure 8 shows Carbon is well distributed in the position where the STEM picture was taken. As can be seen the Carbon is not only detected where the support is but is also homogeneously distributed over all the sample. The STEM laser operates at high energy levels which causes the Carbon of the Graphene to sublime and to be redeposited near to the beam. That would explain the detection everywhere on the sample.
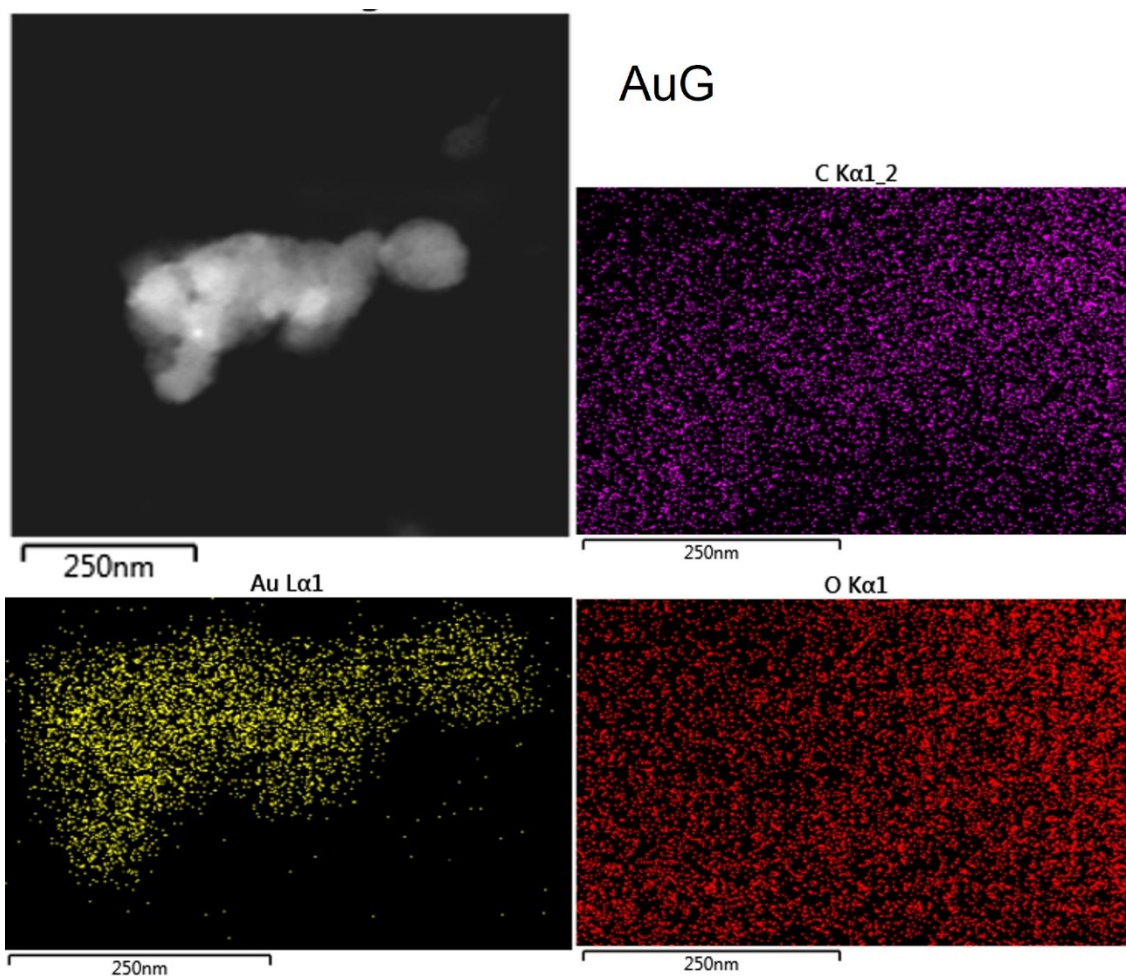
Figure 8 STEM and Elemental Mapping of AuG

Figure 9 shows the STEM pictures and the elemental mapping of AuGS. The Carbon is homogenously detected over the image and not only on the Graphene, due to the previously stated redeposition by the laser. Sulfur is detected only on the Graphene support. The detected Sulfur is evidence of the doping but also evidences the ligands of the Gold Clusters. The Gold signals are only distributed over

the Graphene support and are not loose on the sample. As already mentioned in the previous part, the Gold Clusters are not as homogeneously distributed as the Gold Clusters on undoped Graphene.
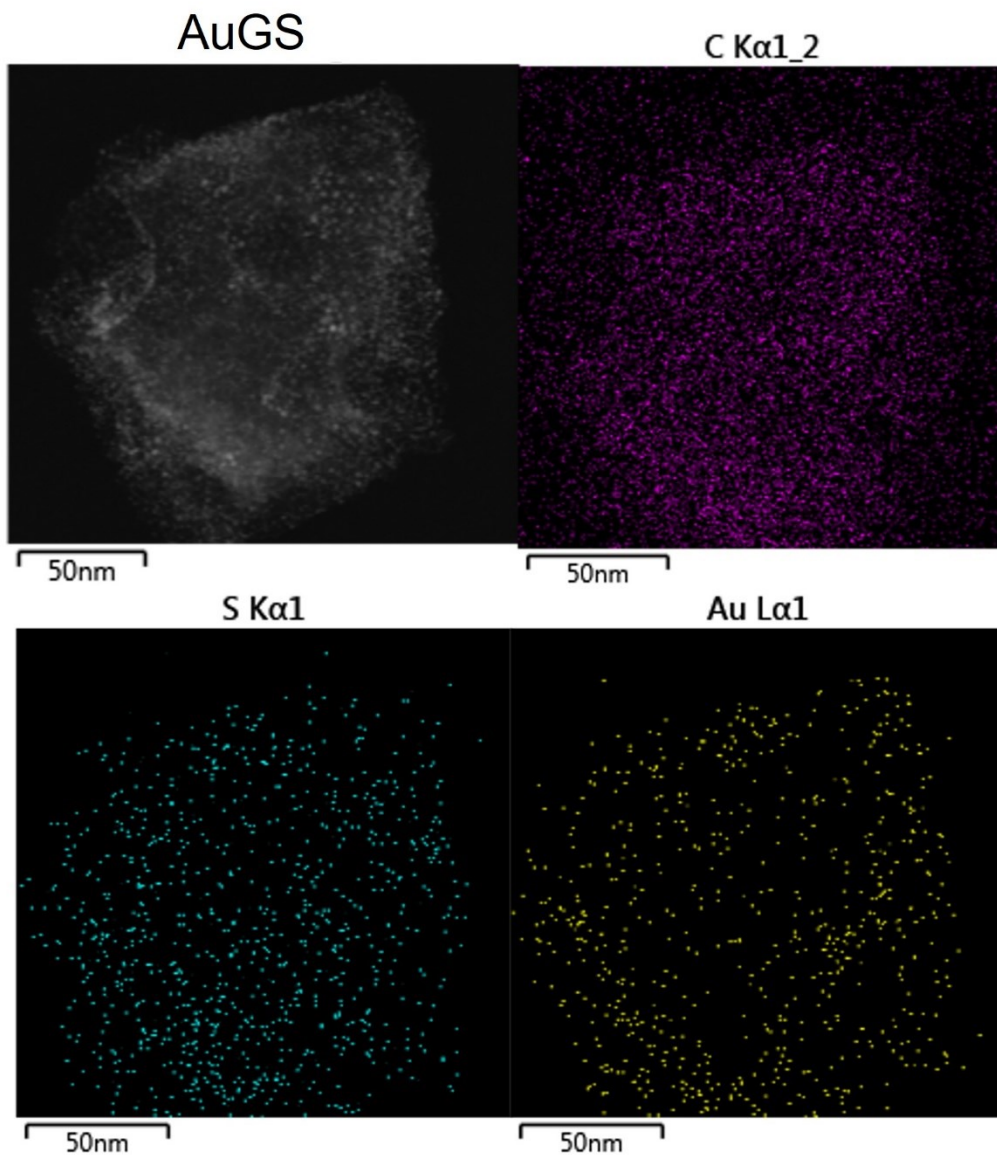

Figure 9 STEM and Elemental Mapping of AuGS

Figure 10 shows the STEM images and elemental mapping of AuGN. This mapping shows the homogeneous distribution of Carbon over the sample, just as with AuG and AuGS. Since the Graphene is doped with Nitrogen it can also be observed, that the Nitrogen is well distributed over the Graphene support. The mapping of Gold and Sulfur shows, that both elements are distributed in the same regions of the sample. This shows the presence of the Thiolate ligands (R-SH) protecting the Gold Cluster. The Gold signals are distributed only over the Graphene support, but some regions show more signals. This can be due to the amorph and more 3-D support or maybe agglomeration of the Nanoclusters.
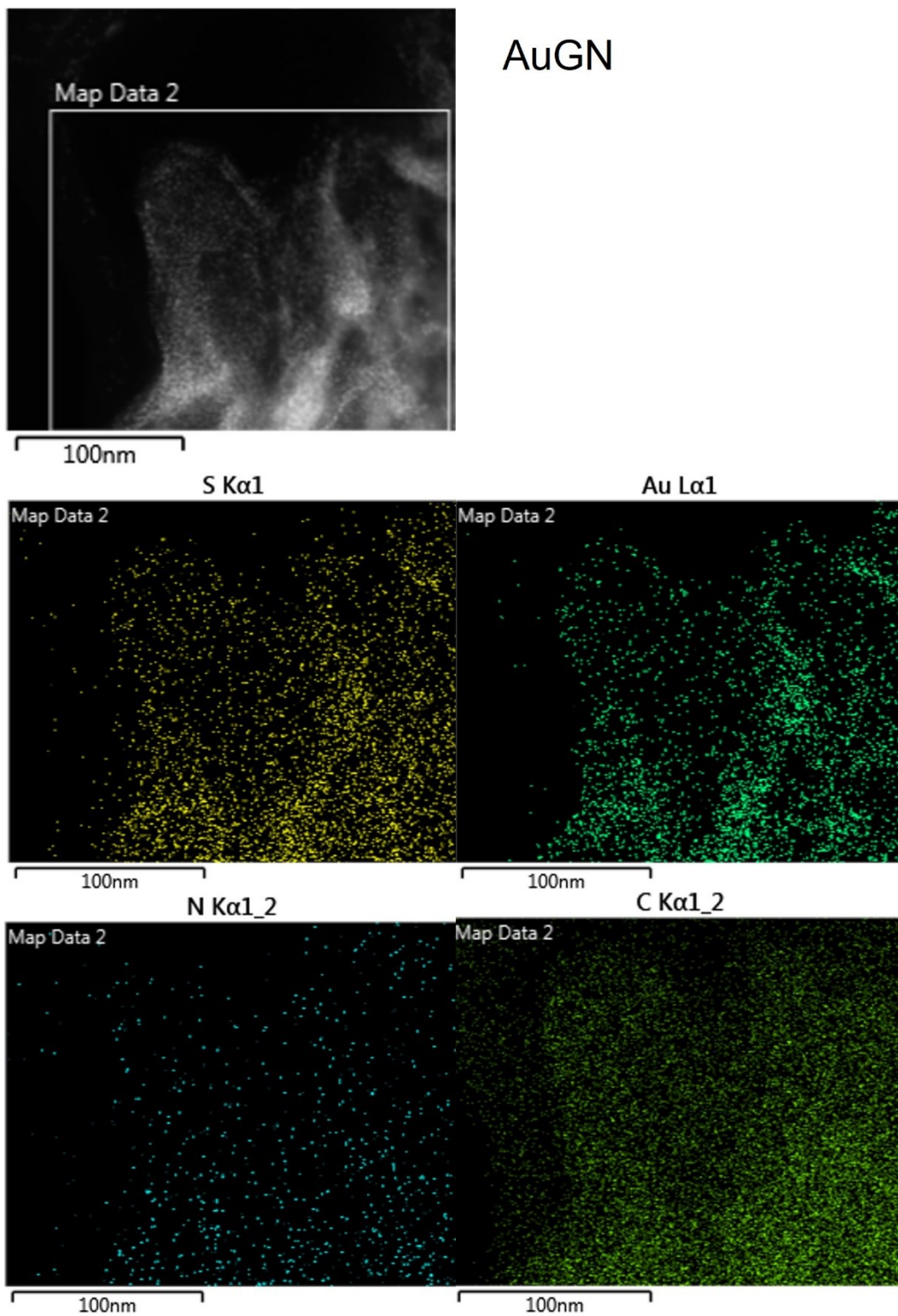
Figure 10 STEM and Elemental Mapping of AuGN

As previously stated in 1.2 the Particle size of the AuNCs is 1nm. To confirm this, the Particle size was calculated using the black and white images obtained by STEM. Due to blurriness and fast decomposition of the material under the electron rays of the STEM Laser not only one Particle size was

obtained, but a Particle size distribution. For AuG an average Particle size of 1.45 nm was obtained with a maximum count of Particles with size slightly larger that 1 nm. For AuGS an average Particle size of 1.13 nm was measured with the highest count of Particles between 0.75 nm and 1.25 nm, matching the estimated Particle size of 1 nm. For AuGN an average Particle size of 1.92 nm was obtained, with a maximum count of Particles at a size between 1 nm and 1.5 nm.
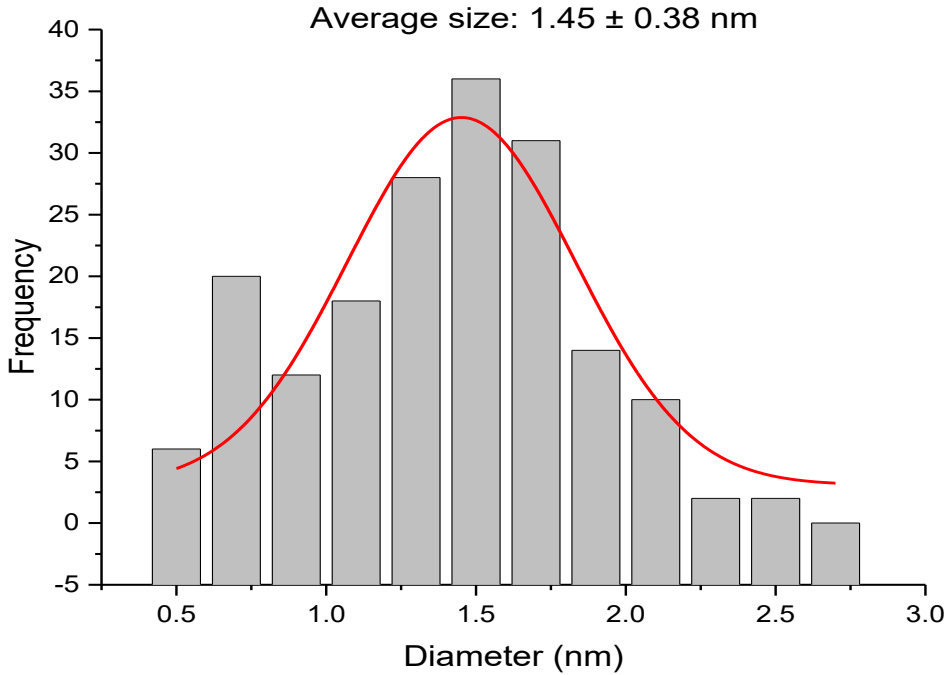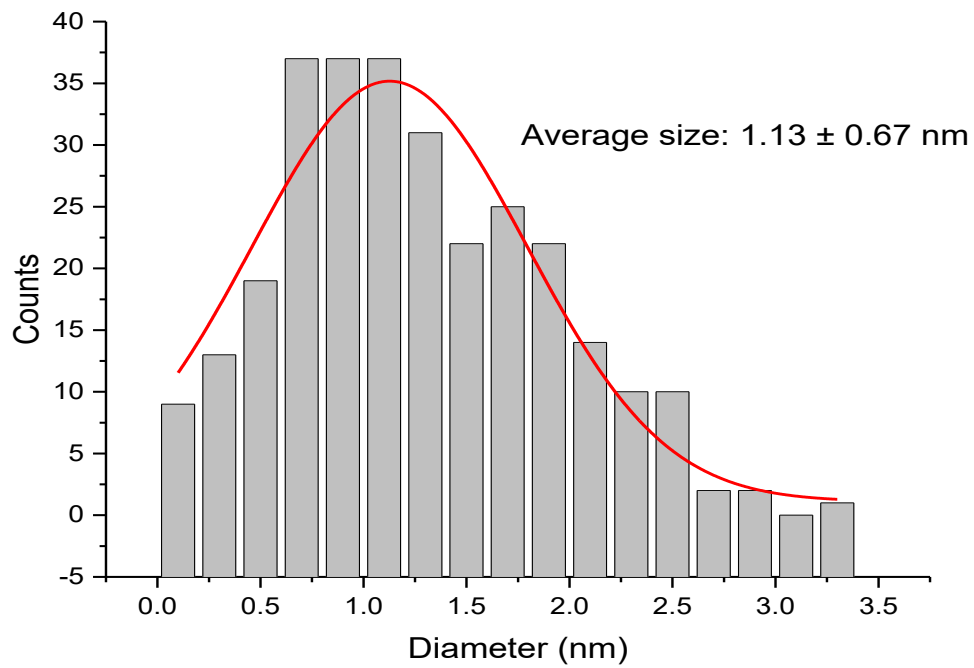

Figure 11 Particle Size Distribution of AuG

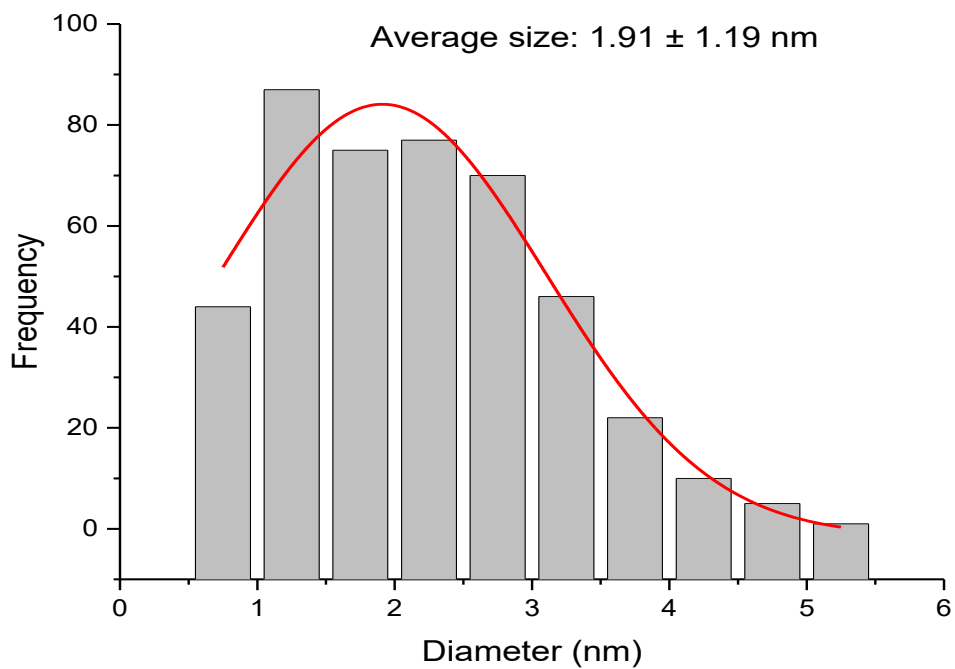*Figure 12 Particle Size Distribution of AuGS*

Figure 13 Particle Size Distribution of AuGN

XRD analysis

As previously mentioned, a PXRD was made of the catalyst powders. Those were compared to a simulated PXRD diffractogram of the AuNCs (Figure 14). The simulated diffractogram displays a typical crystalline signal with little noise and a unique for Au_{25} Clusters peak structure at low diffraction angles. For AuG the signals identifying the Gold Clusters are evident. At higher angles AuG has a higher degree of noise than the simulated Gold attesting the material to be more amorph due to the Graphene. Both AuGN and AuGS are even more amorph than AuG due to the more irregular structure of the Graphenes which were previously attested. AuGN and AuGS show some additional peaks at higher angles and only one single broad peak at lower angles. The broad peak is typical for semicrystalline materials, again attesting the presence of the more amorph Graphene species. The occurrence of additional peaks at higher angles must be investigated further with additional measurements of the Graphene powders under the PXRD.
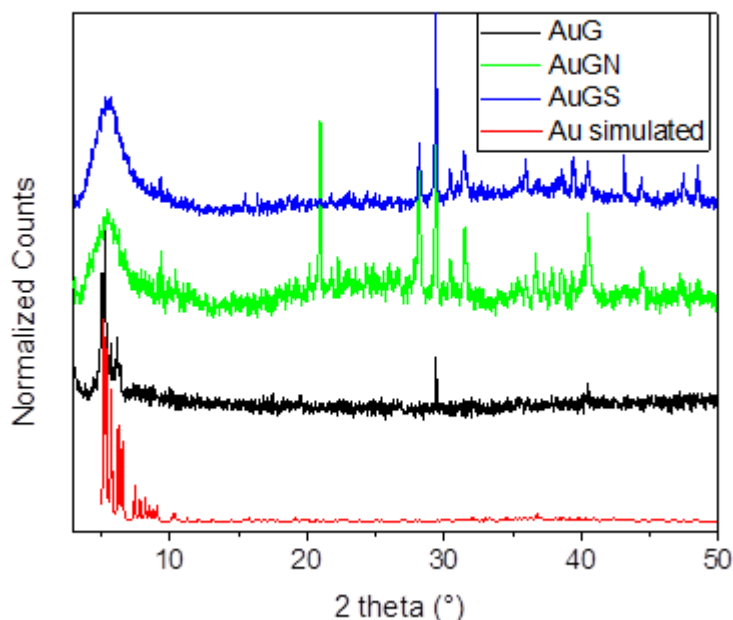

Figure 14 XRD of AuG, AuGN, AuGS and simulated Au Cluster

XPS analysis of Graphene materials:

XPS was used to investigate the distribution and nature of the carbons and the presence and types of dopants (Nitrogen or Sulfur) in the synthetized Graphene materials. In fact, as Carbon is the most common standard for XPS calibration, there are abundant literature data characterizing the binding energies of carbon depending on its hybridization and covalent bonding. Thus, XPS data are the best evidence to support the doping of Graphene.

Figure 15 shows the high-resolution C 1s peak of the three Graphene samples (G, GS and GN). This peak can be deconvoluted in four main components assigned to sp2 C (C=C), sp3 C (C-C), C atoms

bonded to O, N or S and C=O groups centered at 284.5, ~285.6, ~286.8 and ~289.2 eV, respectively.(Xing *et al.*, 2016) Table 2 summarizes the peak positions and atomic percentage of each component. Importantly, the presence of sp3 carbon could be an indicative of residual sp3 carbon from the polysaccharide precursors, suggesting that the transformation of the biopolymer was not 100% completed.
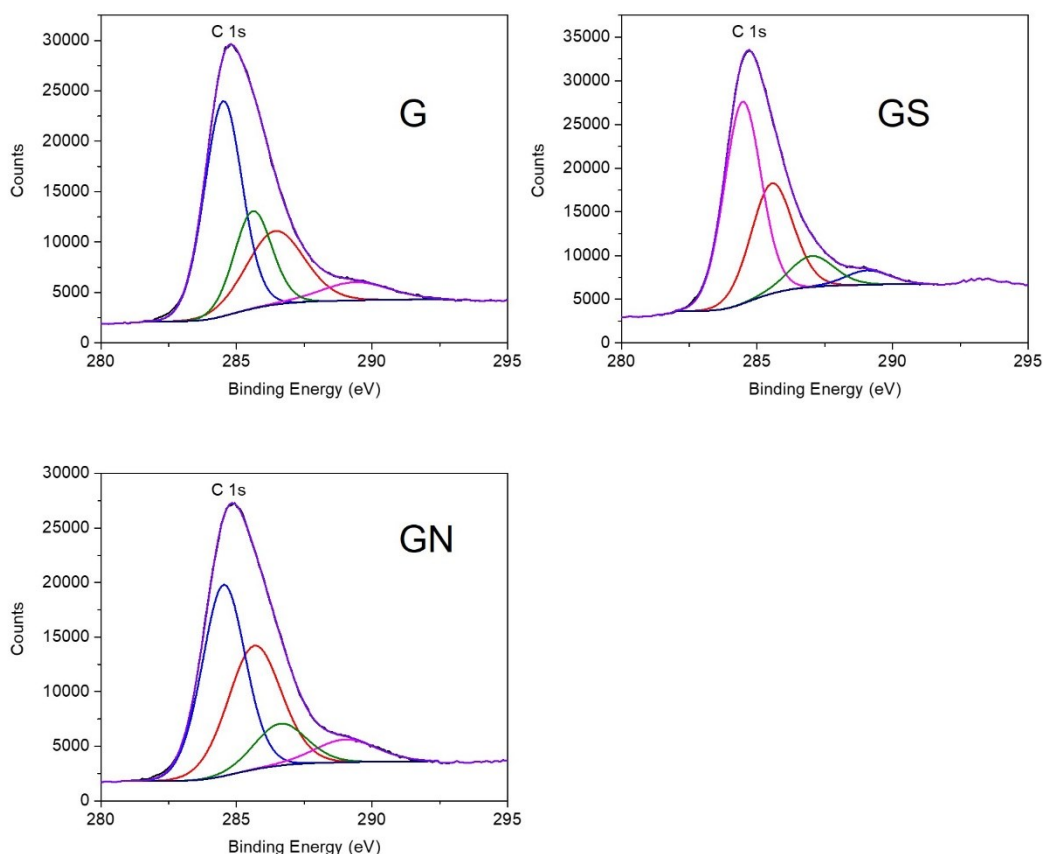

Figure 15 XPS C1s peak of G, GS and GN

Assignment	G		GS		GN	
	Position (eV)	% At. Conc.	Position (eV)	% At. Conc.	Position (eV)	% At. Conc.
C=C (sp2 carbon)	284.5	47.1	284.5	53.0	284.5	44.8
C-C (sp3 carbon)	285.6	21.3	285.6	32.8	285.7	35.8
C-O, C-N or C-S	286.5	24.5	287.0	9.8	286.6	11.8
C=O (carboxyl)	289.4	7.2	289.1	4.4	289.0	7.6

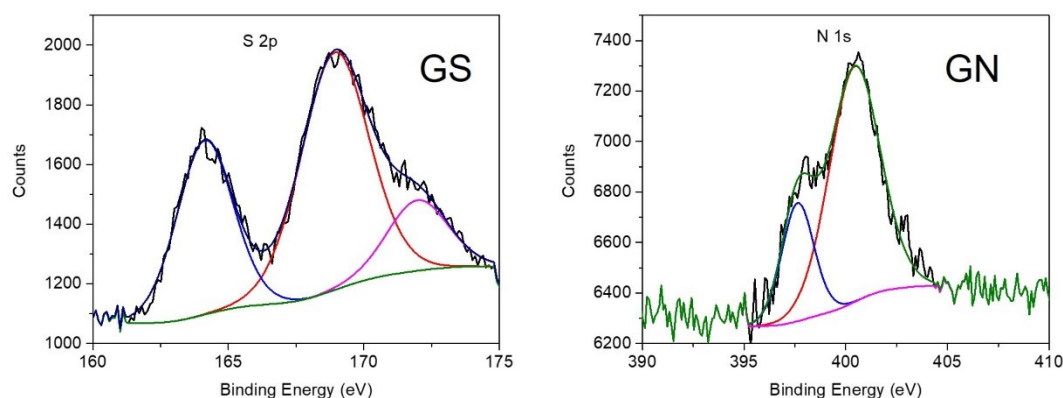Table 2 C 1s Peak Positions and atomic concentration of bond types for G, GS and GN

Figure 16 XPS S 2p peak of GS (left) and N 1s peak of GN (right)

The distribution of N atoms is based on the high resolution XPS N 1s peak for the GN sample (Figure 16 right). The experimental data was deconvoluted to two main components attributed to pyridinic-N (24.16%) and quaternary-, pyrrolic- or graphitic-N (75.8%) N atoms at 387.6 and 400.4 eV, respectively.(Primo *et al.*, 2012; Xing *et al.*, 2016) The amount of Nitrogen doped into the Graphene is 2.5 at% calculated by XPS elemental analysis.

Figure 16 (left) shows the distribution of S atoms based on the high resolution XPS S 2p peak for the GS sample. The S 2p peak was deconvoluted into three components at binding energies of 164.1, 168.9 and 172.0 eV. According to the literature (Choi, Park and Woo, 2011; Dhakshinamoorthy *et al.*, 2015) sulfur was doped into the carbon in two distinct forms, one component corresponding to S atoms bonded to C (–C–S–C–) (~164 eV) and the other two components corresponding to S atoms bonded to C and O (–C–S(O)$_x$–C– ; x = 2–4; ~167.5–171.5 eV), such as in the form of sulfate or sulfonate. In GS, most of the sulfur was doped in the form –C–S(O)$_x$–C– (53.4 % and 14.1 %) and about 32.5% was doped in the form –C–S–C–. The calculated doping concentration of sulfur was 4 at%.

XPS analysis of Au$_{25}$ Graphene materials:

XPS was used to investigate the presence of Au$_{25}$ Clusters on the different Graphene materials and to study the effects of Cluster incorporation on the distribution and nature of the carbons and dopant atoms.

Figure 17 shows the high-resolution C 1s peak of the Au$_{25}$ Graphene samples (AuG, AuGS and AuGN). As explained above for the "nude" Graphene samples, this peak can be deconvoluted in four main components assigned to sp2 C (C=C), sp3 C (C-C), C atoms bonded to O, N or S and C=O groups centered at 284.5, ~285.9 and ~286.9 and ~289.3 eV, respectively.(Xing *et al.*, 2016) However, some differences can be clearly observed after the incorporation of the Au$_{25}$ Clusters; as can be seen in Figure 18 all samples show a significant increase in the atomic percentage of the component assigned to sp3 C (C-C), peak at ~285.9 eV. This effect may be attributed to the presence of the alkyl substituents of the thiolate ligands protecting the Gold Clusters, indicating the prevalence of protecting ligands after incorporation on Graphene.
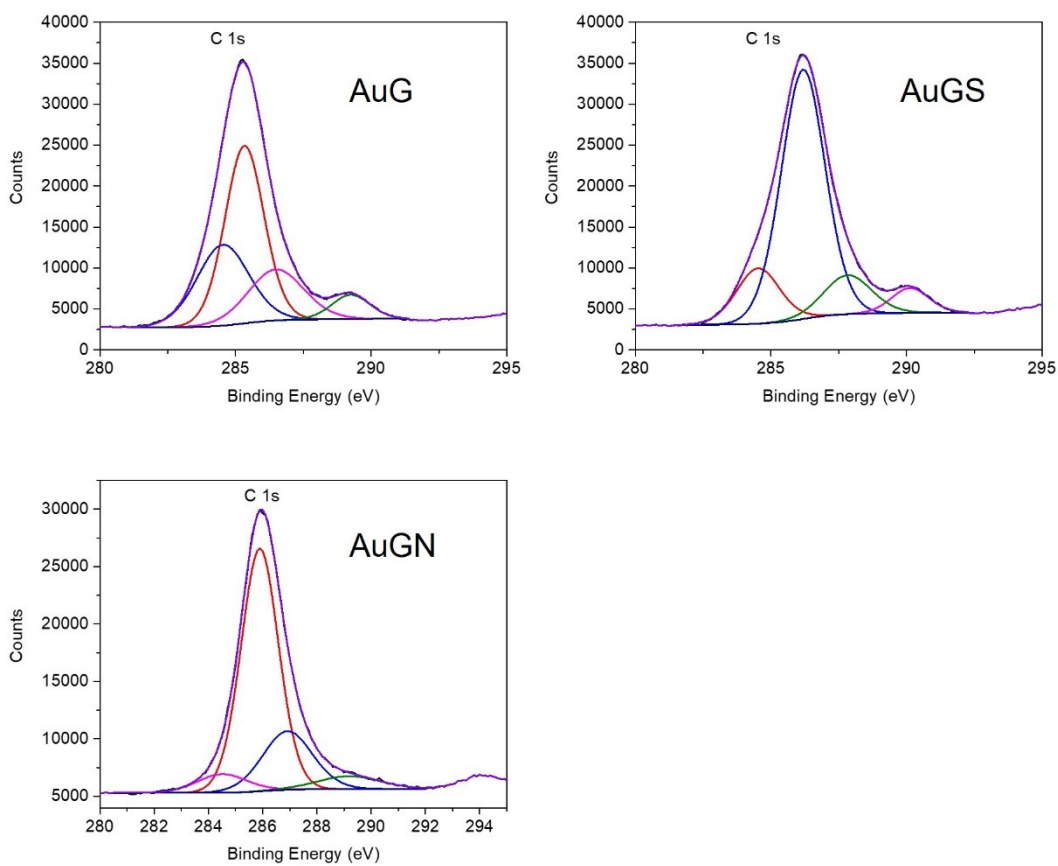
Figure 17 XPS C1s peak of AuG, AuGS and AuGN

Assignment	AuG		AuGS		AuGN	
	Position (eV)	% At. Conc.	Position (eV)	% At. Conc.	Position (eV)	% At. Conc.
C=C (sp2 carbon)	284.5	28.2	284.5	14.9	284.5	6.8
C-C (sp3 carbon)	285.3	46.6	286.2	67.9	285.9	66.2
C-O, C-N or C-S	286.5	19.0	287.8	11.5	286.9	21.2
C=O (carboxyl)	289.3	6.2	290.1	5.7	289.2	5.8

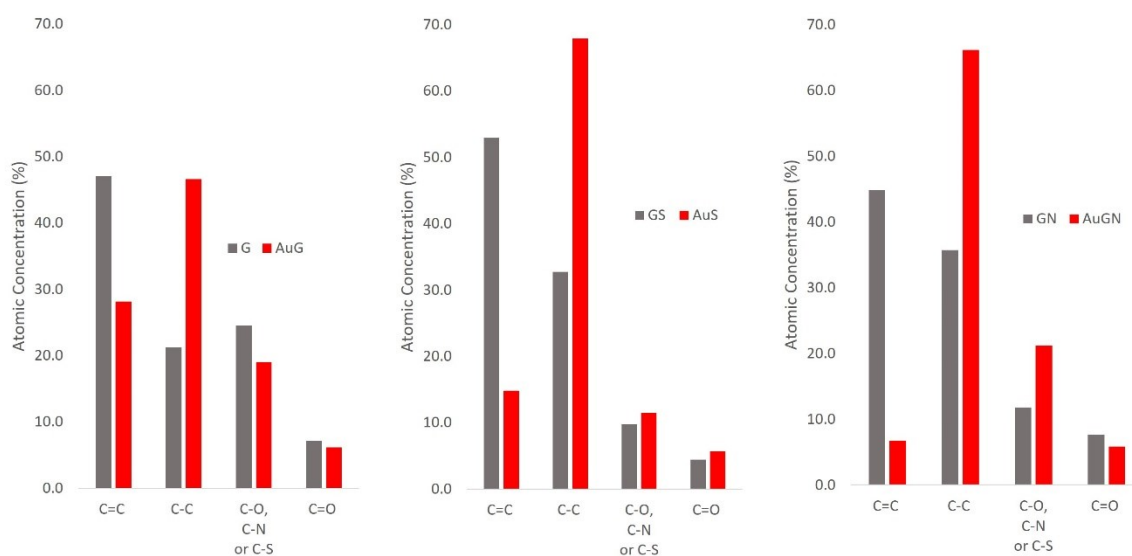*Table 3 C 1s Peak Positions and atomic concentration of bond types for AuG, AuGS and AuGN*

Figure 18 Comparision of Carbon Bond Types of Graphenes with impregnated Graphenes

Figure 19 shows the high-resolution Au 4f peaks of the three Au$_{25}$ Graphene samples (AuG, AuGS and AuGN). The binding energies (BE) of Au 4f$_{7/2}$ and Au 4f$_{5/2}$ are ~84.47 and ~88.26 eV, respectively. It is notable that the BE of Au 4f$_{7/2}$ falls in between the Au(0) BE (84 eV) of a metallic Gold film and the Au(I) BE (85 eV) of Gold Thiolate, confirming the co-existence of Au(0) and Au(I) in the Cluster.(Zhou *et al.*, 2010; Li *et al.*, 2013)
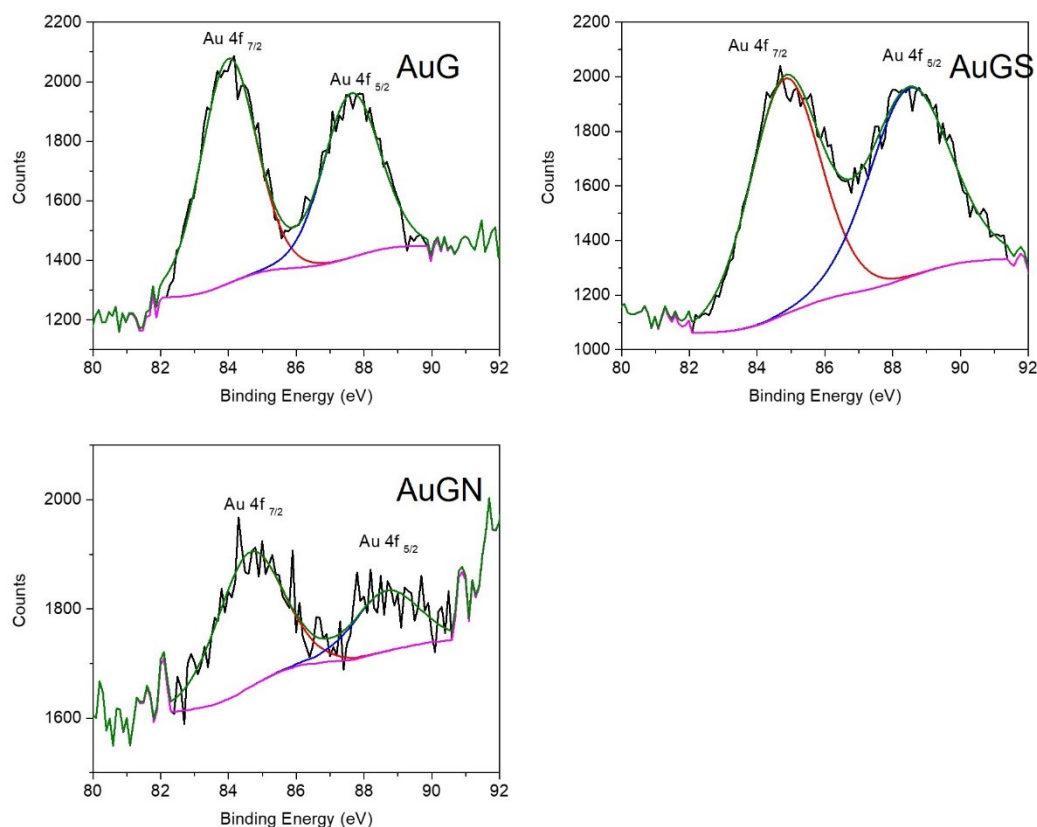
Figure 19 XPS Au 4f peak of AuG, AuGS and AuGN

The S 2p peak of the AuGS sample (Figure 21 left) was deconvoluted into three components at BEs of 164.5, 169.3 and 171.1 eV. As explained above for the GS sample, the first component corresponds to S atoms bonded to C (–C–S–C–) (~164 eV) and the other two components correspond to S atoms bonded to C and O (–C–S(O)x–C–; x = 2–4; ~167.5–171.5 eV). Nevertheless, in the case of AuGS, the first peak can also reveal the presence of the thiolate ligands (R-SH, ~164 eV) protecting the Gold Cluster. According to XPS data, 29.0% of S is bonded to C or in the form of thiol, and 21.8 % and 49.2% of S is in the form –C–S(O)$_x$–C–. In comparison with the bare GS sample (Figure 20 left), that showed 53.4 % and 14.1 % of S in the form of –C–S(O)$_x$–C–, we can conclude that the incorporation of Au$_{25}$ Clusters leads to more oxidized sulfur forms such as sulfate –C–S(O)$_4$–C–.
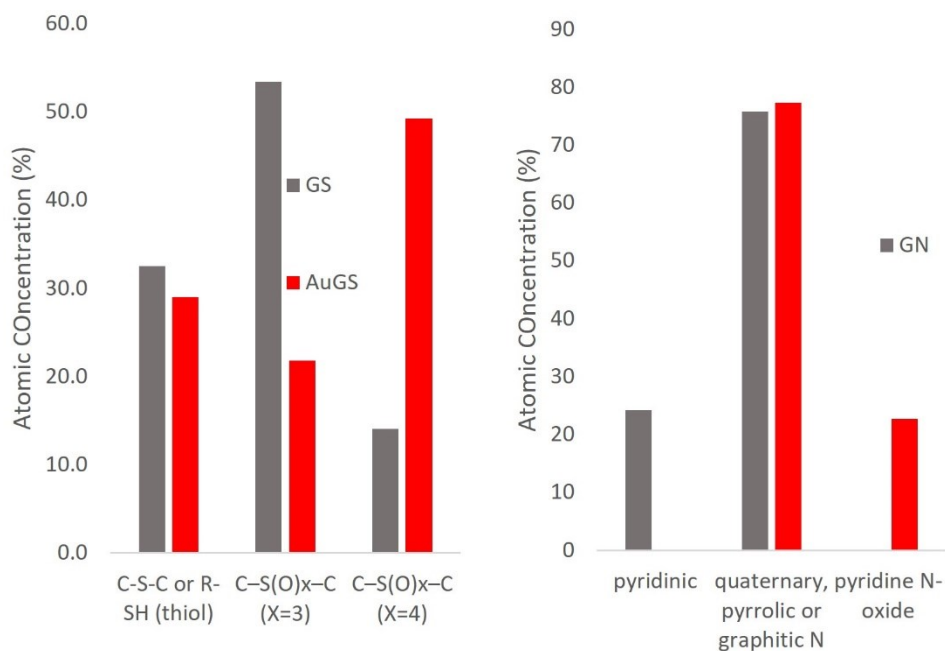
Figure 20 Comparison of Bond Types of Graphenes with impregnated Graphenes

The high resolution XPS N 1s peak of AuGN (Figure 21) was deconvoluted into two components at 400.9 and 403.7 eV. As mentioned above for the GN sample, the peak at ~400 eV corresponds to pyrrolic- or graphitic-N.(Primo *et al.*, 2012; Xing *et al.*, 2016) The component at 404 eV can be attributed to pyridine N-oxide.(Yang *et al.*, 2015) In comparison with the bare GN (Figure 20 right), where the two main components were attributed to pyridinic-N (387.6 eV; 24.16%) and quaternary-, pyrrolic- or graphitic-N (400.4 eV; 75.8%) N atoms, the incorporation of AuNCs leads to the disappearance of pyridinic-N and the appearance of pyridine N-oxide (404 eV; 22.7 %), while maintaining a similar percentage (77.3 %) of quaternary-, pyrrolic- or graphitic-N. Therefore, we can conclude that the incorporation of AuNCs leads to more oxidized N forms. A similar effect was observed for S atoms in the AuGS sample.
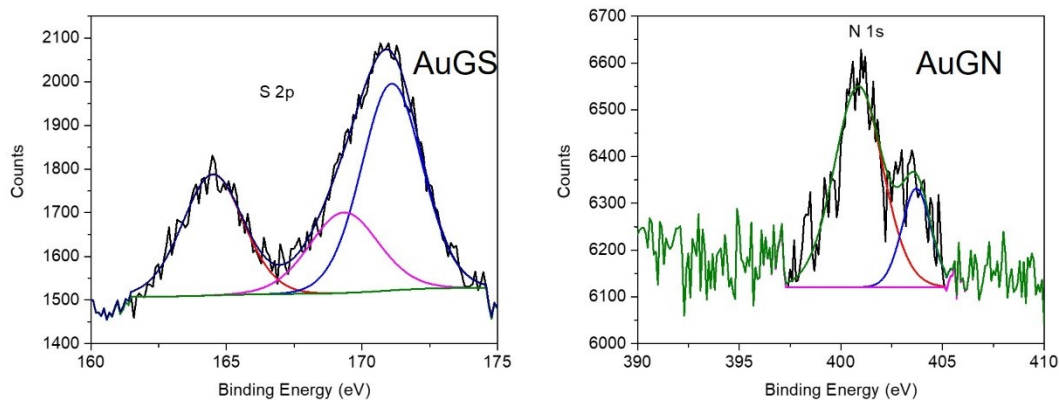

Figure 21 XPS S 2p peak of AuGS (left) and N 1s peak of AuGN (right)

Finally, Table 4 summarizes the atomic percentage of each element for all the samples, it can be seen that the % of doping atoms decreases after incorporation of AuNCs, but this may be just a "masking" effect since XPS is a surface analysis technique and the deposition of Au_{25} Clusters on the Graphene's surface may influence the quantification of the different doping elements

Sample	G	AuG	GN	AuGN	GS	AuGS
Element	Atomic Concentration in %					
C	100.0	99.8	97.6	98.4	96.0	97.8
Au		0.2		0.1		0.3
N			2.5	1.5		
S					4.0	1.9

Table 4 Atomic percentage of each element for each sample

3.1.3. Optical Property Characterization

To analyze if the impregnation of the Gold on the different support species caused a permanent change in the structure of the AuNCs for example a change of the shape or agglomeration a UV-Vis Spectra of the AuNCs was made.
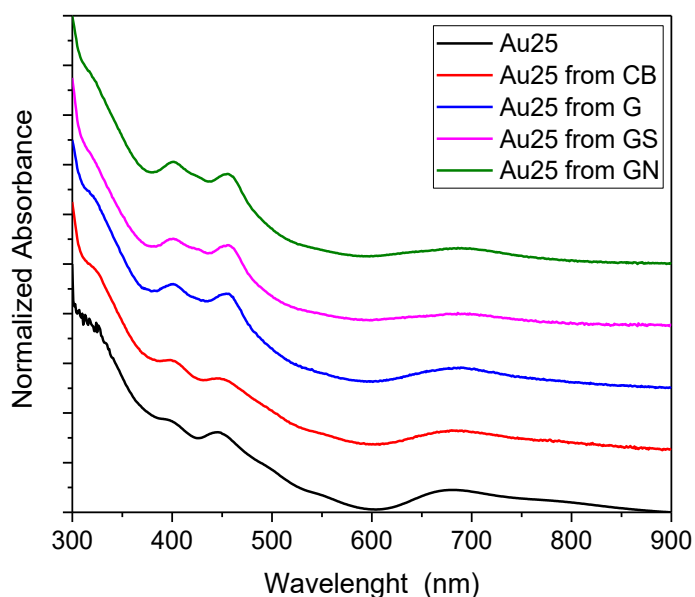

Figure 22 UV-Vis Spectra of Au_{25} before and after impregnation on support

In Figure 22 all characteristic peaks for Au_{25} at the wavelength 400, 445 and 685 nm can be seen.(Zhao *et al.*, 2018) The multiple molecular-like transitions in the absorption spectrum are ascribed to the strong quantum size effects of Au_{25} NCs, which are different from the surface plasmon resonance at approximately 520 nm for large Gold NPs.(Wu and Jin, 2021) This leads to the conclusion that the Gold Clusters do not change their structures during impregnation and that they do not transform to large Gold NPs via aggregation processes.

3.2. Electrocatalytic CO_2 reduction tests

3.2.1. Activity and Selectivity

CAs were made to analyze the activity and selectivity of the catalysts. The current density over the timespan of 30 min was then obtained (Figure 23). AuG and AuGN show the worst activity compared to the tested materials. A higher activity has AuGS but is still lower than the blank experiment which was only made with the bare Carbon Paper electrode. The highest current density was obtained with CB but it can be seen, that the current density decreases significantly over the short period of time, suggesting a low catalyst stability.
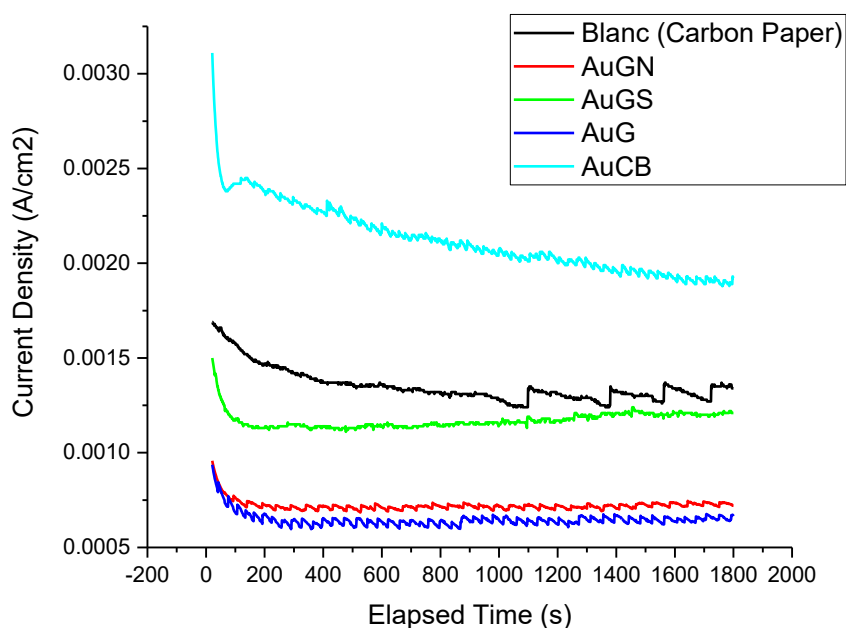

Figure 23 Current density of different samples compared to a blank

After each CA the gas phase of the reactor was tested with GC to quantify the gaseous products. Then the FEs were calculated and plotted in Figure 24. In the blank experiment, only a small amount of CO was obtained at higher voltages and the main product was H_2. The catalysts containing AuNCs show a higher selectivity towards CO which confirms the extensively documented ability of AuNCs to reduce CO_2 to CO.

The best FEs even at lower overpotentials, were obtained by AuCB with a maximum efficiency at -0.7 V vs RHE. The best performances of the Gold on Graphene catalysts were obtained by AuGS with a maximum efficiency of 50% of CO production at a Voltage of -0.7 and -0.8 V vs RHE. The other catalysts have an unsatisfactory performance with the best FE efficiency of AuGN being 13.5 % and of AuG being 32% at-0.9V vs RHE.
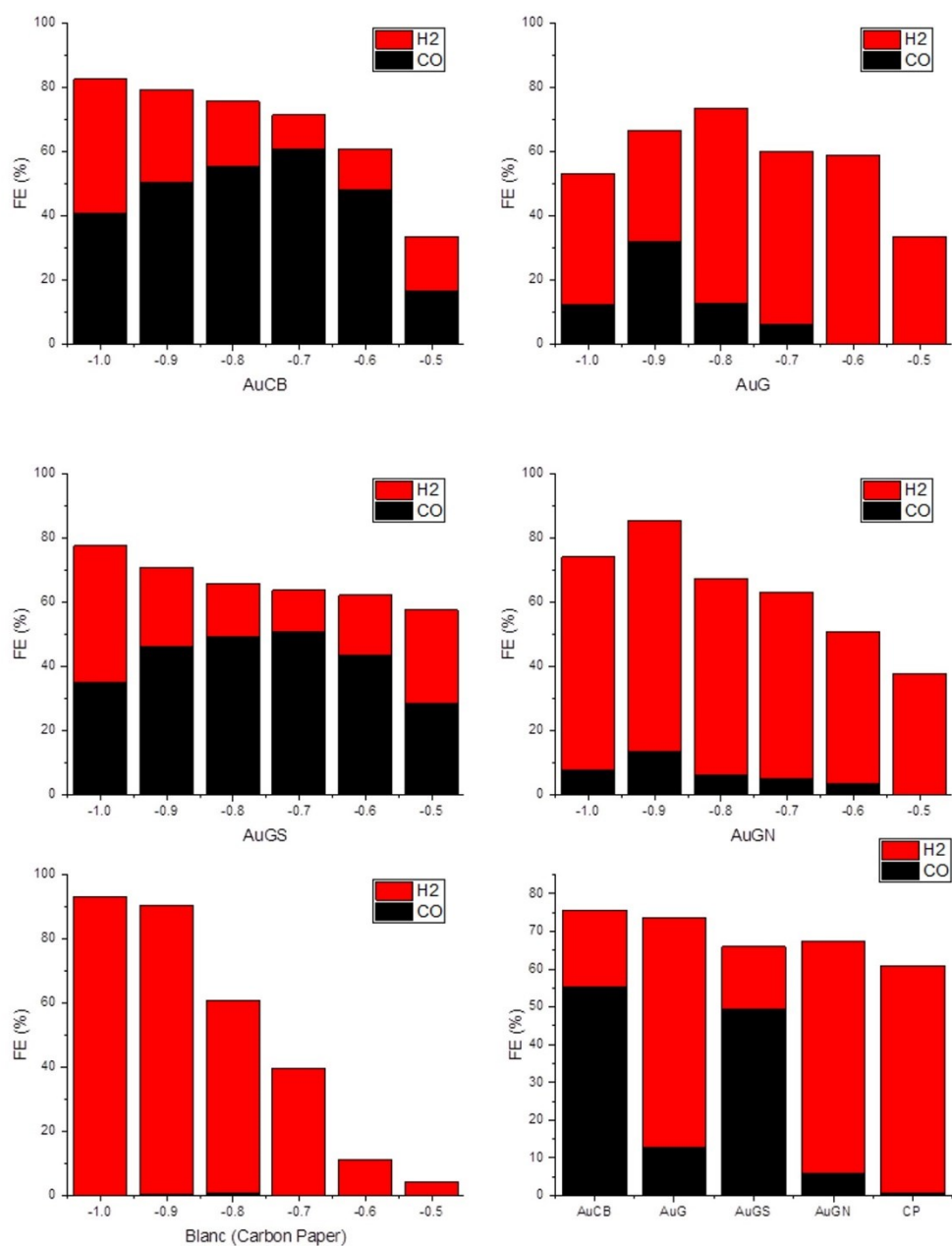
Figure 24 Comparison of FE of all materials and Carbon Paper as blank at potentials ranging from -0.5 V to -1.0 V vs RHE. As well as the comparison of FE of all tested materials at a potential of 0.8 V vs RHE (bottom right)

To test if the catalysts produce a liquid product, liquid NMR was tested with the Gold impregnated on Graphenes and Carbon Black. The electrolyte was not exchanged in between the CAs leading to an accumulation of the products in the liquid phase of the reactor. That is also the reason why the findings can only be used to determine the best catalyst qualitatively and not quantitatively. The NMR analysis showed that the only liquid product is Formic Acid. As can be observed in Figure 25 the highest share of Formic Acid has AuGS. Closely followed by AuCB. Whereas AuGN and AuG have a bad activity towards the formation of Formic Acid.
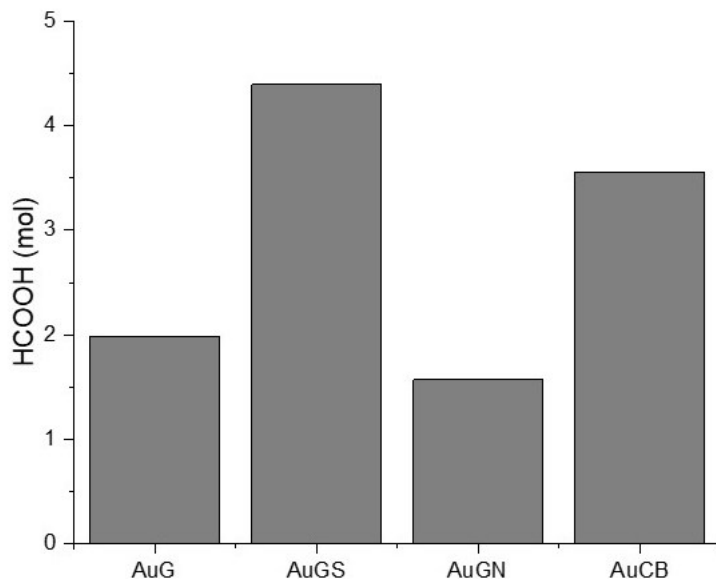
31

Figure 25 Accumulated Quantity of Formic Acid produces after CAs at different potentials

It is of interest if a higher current towards the formation of CO is obtained at a specific potential. Therefore, the partial CO current density was plotted as a function of the potential vs. RHE. As it can be seen in Figure 26, at low overpotentials only a low current density is obtained. For AuG and AuGN there is a peak in performance at a potential of -0.9V. For AuGS and AuCB the highest partial current is given at a potential of -0.9 V vs RHE.
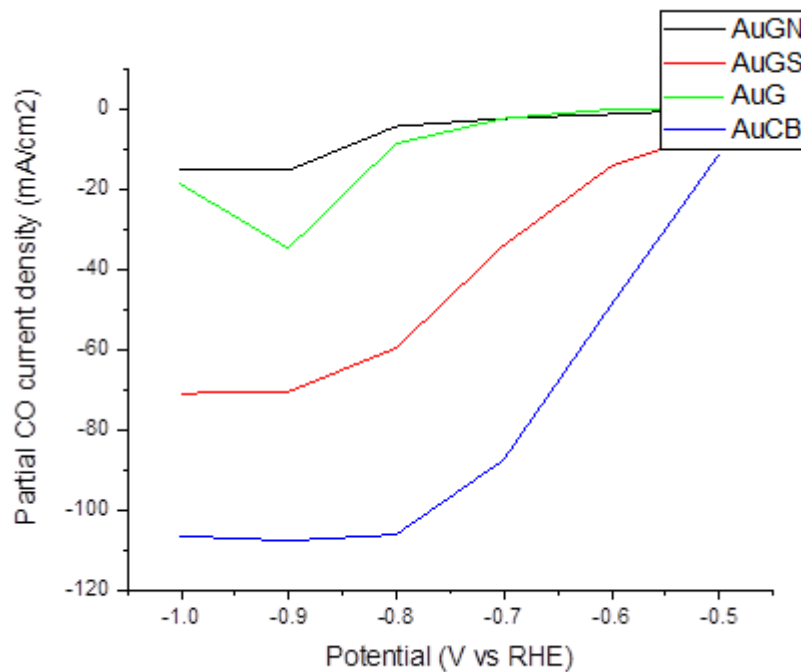

Figure 26 Partial CO Current Density

3.2.2. Stability

As already observed in 3.2.1 the current density of AuCB already decreases at short periods of time, leading to the assumption that this material, has a high degradation rate. To further compare the materials in respect to their stability, CVs were made before and after the six CAs which were done under different potentials. In Figure 27 the full CVs of AuG and AuCB are shown. AuCB shows a high maximum current density at about -0.005 A/cm^2 at the beginning of the experiments and a significantly lower current density between -2 mA/cm^2 and -3 mA/cm^2 after the CAs.

To compare the other catalysts and for clarity only the first cycle of the respective CVs is shown in Figure 28. AuGN has a big decrease in current density going from -2.5 mA/cm^2 to -1.5 mA/cm^2. Also, a decrease in current density can be observed for AuGS having a current density of -2.75 mA/cm^2 at the beginning and a current density of -2 mA/cm^2 at the end. The least decrease of maximum current density can be seen by AuG which has a current density of -2.25 mA/cm^2 before the CAs and of -1.75 mA/cm^2 after them. With a decrease of 1 mA/cm^2 AuCB is the least stable of the tested catalysts and with a decrease of only 0.5 mA/cm^2 AuG has the best stability.
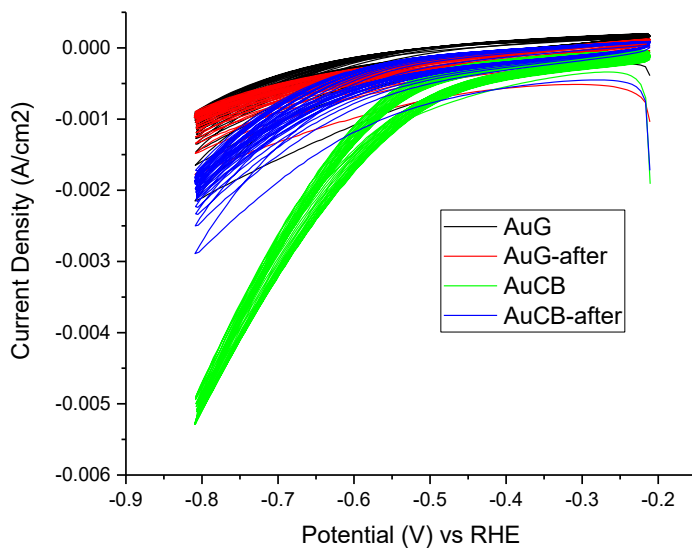

Figure 27 CVs to compare activity before and after 3 h of Chronoamperometries for AuG and AuCB
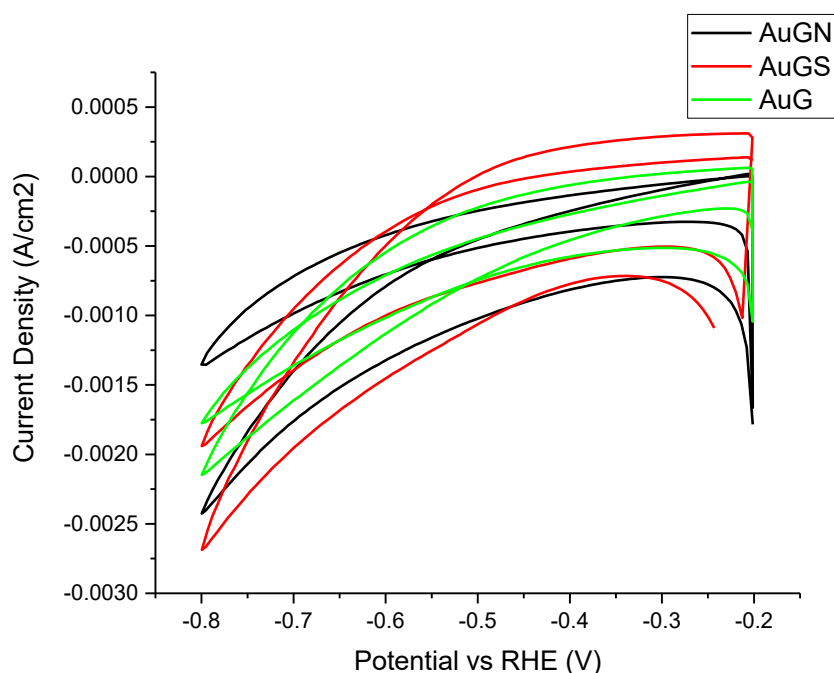
Figure 28 CVs to compare activity before and after CAs (only Single Voltammetries shown for clarity)

3.2.3. Conductivity properties

To explain the difference in activities of the different catalysts some measurements with EIS were made to obtain the different resistances of the parts that play a role during the reaction.

As can be seen in Figure 29 there are only parts of the characteristic half circles observable, leading to the conclusion that the impedance due to Hemholtz double layer is minimal compared to the other resistances taking part in this reaction. The right end of the half circle, is the resistance of the electrode and the impedance of the Helmholtz layer, combined. As you can see, the resistances of the different catalysts are quite similar between 30 kΩ and 40 kΩ. A more obvious difference between the catalysts, is the line after the half circle fragment, which is called Warburg diffusion element. The steeper the Warburg element is, the less diffusion resistance is there. A maximum of diffusion resistance is obtained at a 45° angle. As can be seen in Figure 29 (right) which is a closeup to the impedance part, AuGN has the highest diffusion resistance. AuG shows a slightly better diffusion resistance. Looking at the whole EIS measurements it can be seen that AuGS has the second highest diffusion conductivity. AuCB has the best diffusion properties of all the tested materials. This leads to the conclusion that the diffusion of ions, CO and products towards and from the catalysts active sites is limited in the catalysts which have Graphene as Support. Similar results were also obtained at the potential -0.5 observable at Figure 31 in the Appendix.
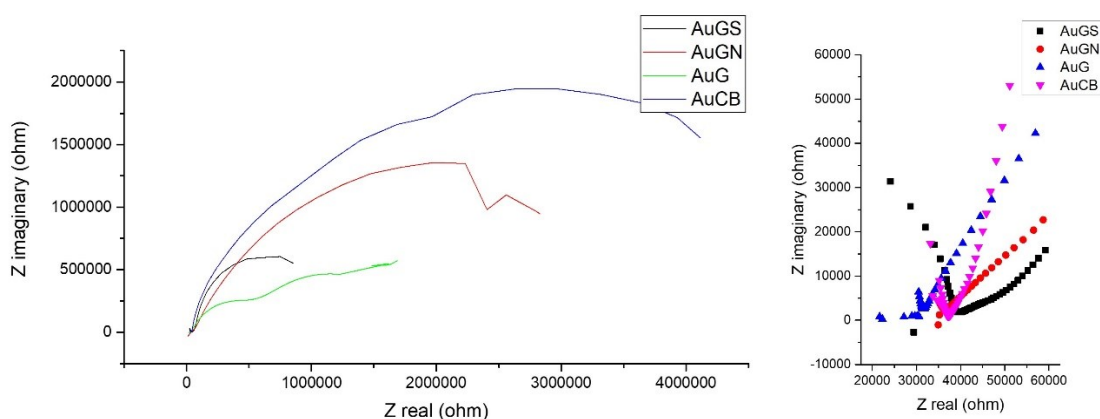
Figure 29 EIS at a Potential of -0.6 V vs RHE

4. Conclusions

The purpose of this work was to improve catalysts consisting of Gold Nanoclusters and their support by investigating and analyzing the benefits of heteroatom-doped Graphene as support. Other goals were to improve the catalyst stability, the performance and the synergy between active catalyst and supporting carbon material.

To do so, a variety of carbon materials where impregnated with AuNCs and analyzed for its physical and electrochemical abilities. Structural characterization showed that the different Graphenes are different in morphologies. AuG has a well-defined hexagonal structure whereas doped Graphenes are more amorphous. The most amorphous Graphene that was analyzed within this work, is GS.

When the different Graphene species were then impregnated with the Gold, no change in the electronic structure of the Graphenes were witnessed by Raman Spectra. Even though the XPS Analysis showed an increase of sp3 (C-C) bindings, after the incorporation of the AuNCs, but this can be attributed to the presence of the alkyl substituents of the thiolate ligands protecting the Gold Clusters. XPS also showed, that the incorporation of Au_{25} into the doped Graphenes, lead to some oxidation of the dopants. For example, some sulfur compounds were oxidized to sulfates.

The morphology before and after the impregnation of the Graphenes with the Gold Clusters was analyzed with TEM. No difference in morphology of the Graphenes before and after the impregnation could be identified. The AuNCs were differently well distributed on the Graphenes. Meaning, AuG had evenly distributed Gold Particles due to its homogenous structure, whereas in AuGS the Gold Particles seemed more randomly distributed. With the help of STEM images the Particles size distribution was calculated and led to the conclusion that the Clusters have an average size between 1.13 nm and 1.91 nm. But it is supposed, that the difference of the Particle size is only due to measurement uncertainties and blurriness of the STEM images, since the UV-Vis spectra doesn't show a change in the structure of the Gold Particles after impregnation.

AuCB offers the highest overall activity and has also the highest activity towards CO formation as can be seen by comparing the total current density and the partial CO current density of the different materials. It doesn't only have the highest activity, when looking at the FEs AuCB also has the highest selectivity towards CO formation. AuCB had a FE towards CO formation of 61% at 0.7 V followed by AuGS with a FE of 50%.

To identify the reasons of why there are differences in activity, conductivity measures by doing EIS were made. These showed that the main resistance in all tested catalysts is caused by diffusion limitation. This suggests that the active sites aren't easily accessible for reactants and products. EIS measurements showed that AuCB had the lowest diffusion resistance, followed by AuGS. This would explain their overall high activity. These two materials are more amorph and with that have a more open structure and probably a more accessible surface which would explain the lower diffusion resistance. With CO_2 being a bigger molecule than H_2O or H_2 the steric effects during diffusion processes and speed play a significant role within the selectivity of reactions. Graphene having sheets that overlay each other it might be possible that CO_2 molecules have steric problems accessing the Gold Nanoclusters, leading to a lower active surface of the Graphene and a lower conversion rate. In comparison AuCB has a very open structure and leading to high accessibility and a higher activity. When only looking at the activity and selectivity the existing data suggests that AuCB is the material that performs the best under the tested catalysts. In the past AuNPs were already tested on a kind of Graphene, namely the GNRs that were mentioned in Chapter 1.4 which showed a really good performance towards CO_2 reduction. It is supposed that the reason why there was such a big difference between the Gold Nanoclusters on Graphenes, which were analyzed in this work and the Gold Nanoparticles on GNR is the porosity of GNRs.

Another important property of catalysts is their stability. Comparison of the CVs before and after multiple CAs suggest that the tested catalysts which are based on Graphene support have a higher stability than the Gold Clusters supported on CB. This might be due to the d-π bonding which stabilizes the AuNCs on the Graphenes. Whereas AuG already showed in short CAs of only 30 min at a Voltage of 1.4 V a decrease of current density. This concludes that AuCB might have a good Activity and Selectivity compared to AuNCs on Graphenes, but lacks Stability.

In future should be investigated on why AuCB lacks stability. Many possible ways are possible: Does the support degrade, are the Goldclusters detaching of the CB, are the Goldclusters changing their shape and many more. With that knowledge an improvement of the catalysts would be possible. For example CB could be doped with heteroatoms to provide stability or the Graphenes production could be changed to improve the diffusion capabilities.

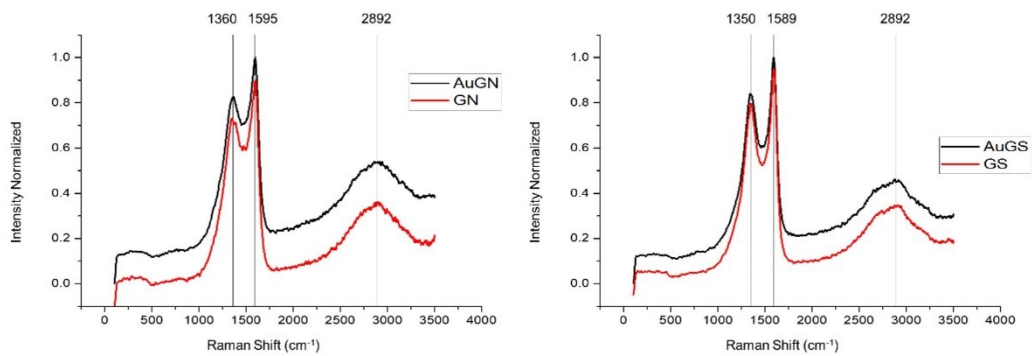# 5. Annex

5.1. Additional Graphics

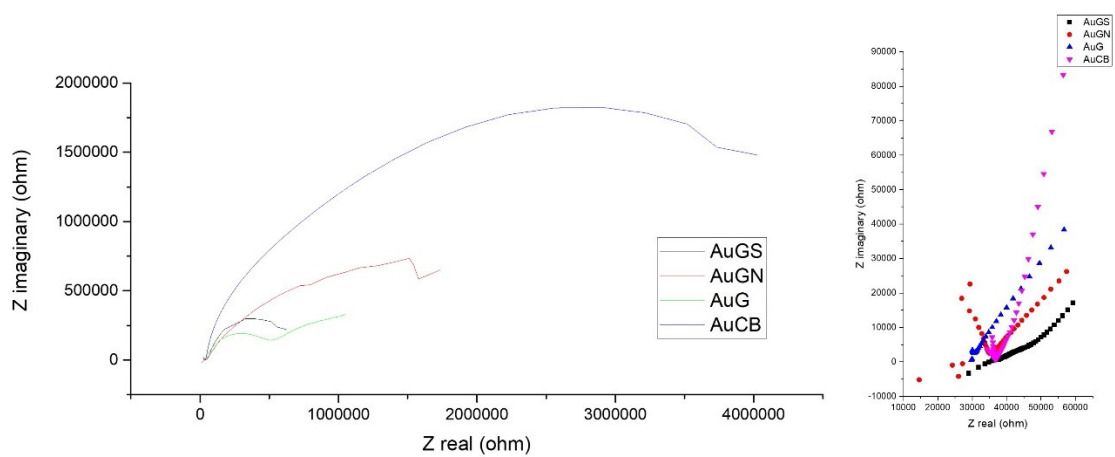*Figure 30 Raman Spectra of GN and AuGN (left) and GS and AuGS (right)*

Figure 31 EIS at a Potential -0.5 vs RHE

5.2. References

Arrhenius, S. (1896) *On the Influence of Carbonic Acid in the Air upon the Temperature of the Ground*, *Philosophical Magazine and Journal of Science Series*. Available at: http://www.globalwarmingart.com/.

Bharti, S.K. and Roy, R. (2012) 'Quantitative 1H NMR spectroscopy', *TrAC - Trends in Analytical Chemistry*, pp. 5–26. Available at: https://doi.org/10.1016/j.trac.2012.02.007.

Cai, X. *et al.* (2022) 'Catalytic Conversion of CO2over Atomically Precise Gold-Based Cluster Catalysts', *ACS Catalysis*. American Chemical Society, pp. 10638–10653. Available at: https://doi.org/10.1021/acscatal.2c02595.

Candu, N. *et al.* (2019) 'Nitrogen-doped graphene as metal free basic catalyst for coupling reactions', *Journal of Catalysis*, 376, pp. 238–247. Available at: https://doi.org/10.1016/j.jcat.2019.07.011.

Choi, C.H., Park, S.H. and Woo, S.I. (2011) 'Heteroatom doped carbons prepared by the pyrolysis of bio-derived amino acids as highly active catalysts for oxygen electro-reduction reactions', *Green Chemistry*, 13(2), pp. 406–412. Available at: https://doi.org/10.1039/C0GC00384K.

EEA (European Environment A) (2008) *Climate change targets: 350 ppm and the EU two-degree target*.

Dhakshinamoorthy, A. *et al.* (2015) 'Sulphur-doped graphene as metal-free carbocatalysts for the solventless aerobic oxidation of styrenes', *Catalysis Communications*, 65, pp. 10–13. Available at: https://doi.org/10.1016/j.catcom.2015.02.018.

Diehl, B. (2008) *Fundamentals and Techniques; Principles in NMR Spectroscopy*.

Harvey, D. (2000) *Modern analytical chemistry*. McGraw-Hill.

Keeling, C.D. (1997) *Climate change and carbon dioxide: An introduction*. Available at: www.pnas.org.

Li, L. *et al.* (2013) 'Effect of polymer ligand structures on fluorescence of gold clusters prepared by photoreduction', *Nanoscale*, 5(5), pp. 1986–1992. Available at: https://doi.org/10.1039/C2NR33693F.

Lindsey, R. (2022) *Climate Change: Atmospheric Carbon Dioxide*. Available at: https://www.climate.gov/news-features/understanding-climate/climate-change-atmospheric-carbon-dioxide (Accessed: 8 January 2023).

McCreery, R.L. (2005) 'Raman Spectroscopy for Chemical Analysis', in *Raman Spectroscopy for Chemical Analysis*. John Wiley & Sons, Inc., pp. i–xxiv. Available at: https://doi.org/10.1002/0471721646.fmatter.

Niu, S. *et al.* (2020) 'How to Reliably Report the Overpotential of an Electrocatalyst', *ACS Energy Letters*. American Chemical Society, pp. 1083–1087. Available at: https://doi.org/10.1021/acsenergylett.0c00321.

Pei, E. al (2021) *A brief review of electrocatalytic reduction of CO2 - Materials, reaction conditions, and devices*. Available at: https://doi.org/10.1002/ese3.935.

Primo, A. *et al.* (2012) 'From biomass wastes to large-area, high-quality, N-doped graphene: Catalyst-free carbonization of chitosan coatings on arbitrary substrates', *Chemical Communications*, 48(74), pp. 9254–9256. Available at: https://doi.org/10.1039/c2cc34978g.

Rogers, C. *et al.* (2017) 'Synergistic Enhancement of Electrocatalytic CO2 Reduction with Gold Nanoparticles Embedded in Functional Graphene Nanoribbon Composite Electrodes', *Journal of the American Chemical Society*, 139(11), pp. 4052–4061. Available at: https://doi.org/10.1021/jacs.6b12217.

Rostron, P., Gaber, S. and Gaber, D. (2016) 'Raman Spectroscopy Review', *Article in International Journal of Engineering and Technical Research*, (6), p. 50. Available at: www.erpublication.org .

Stevie, F.A. and Donley, C.L. (2020) 'Introduction to x-ray photoelectron spectroscopy', *Journal of Vacuum Science & Technology A*, 38(6), p. 063204. Available at: https://doi.org/10.1116/6.0000412.

Wang, G. *et al.* (2021) 'Electrocatalysis for CO2conversion: From fundamentals to value-added products', *Chemical Society Reviews*. Royal Society of Chemistry, pp. 4993–5061. Available at: https://doi.org/10.1039/d0cs00071j.

Wang, J. *et al.* (2019) ' Linkage Effect in the Heterogenization of Cobalt Complexes by Doped Graphene for Electrocatalytic CO 2 Reduction ', *Angewandte Chemie*, 131(38), pp. 13666–13673. Available at: https://doi.org/10.1002/ange.201906475.

Wu, Z. and Jin, R. (2021) *Atomically Precise Metal Nanoclusters Synthesis Lectures on Mobile and Pervasive Computing Synthesis Lectures on Materials and Optics Atomically Precise Metal Nanoclusters*.

Xing, Z. *et al.* (2016) 'One-pot hydrothermal synthesis of Nitrogen-doped graphene as high-performance anode materials for lithium ion batteries', *Scientific Reports 2016 6:1*, 6(1), pp. 1–10. Available at: https://doi.org/10.1038/srep26146.

Yang, Z. *et al.* (2015) 'In situ incorporation of a S, N doped carbon/sulfur composite for lithium sulfur batteries', *RSC Advances*, 5(95), pp. 78017–78025. Available at: https://doi.org/10.1039/C5RA15360C.

Yau, S.H., Varnavski, O. and Goodson, T. (2013) 'An ultrafast look at Au nanoclusters', *Accounts of Chemical Research*, 46(7), pp. 1506–1516. Available at: https://doi.org/10.1021/ar300280w.

Zhang, H. *et al.* (2019) 'A Graphene-Supported Single-Atom FeN5 Catalytic Site for Efficient Electrochemical CO2 Reduction', *Angewandte Chemie - International Edition*, 58(42), pp. 14871–14876. Available at: https://doi.org/10.1002/anie.201906079.

Zhao, S. *et al.* (2018) 'Influence of Atomic-Level Morphology on Catalysis: The Case of Sphere and Rod-Like Gold Nanoclusters for CO2 Electroreduction', *ACS Catalysis*, 8(6), pp. 4996–5001. Available at: https://doi.org/10.1021/acscatal.8b00365.

Zhou, C. *et al.* (2010) 'Luminescent gold nanoparticles with mixed valence states generated from dissociation of polymeric Au(I) thiolates', *Journal of Physical Chemistry C*, 114(17), pp. 7727–7732. Available at: https://doi.org/10.1021/JP9122584/ASSET/IMAGES/LARGE/JP-2009-122584_0002.JPEG.

Zhu, M. *et al.* (2008) 'Correlating the crystal structure of A thiol-protected Au25 cluster and optical properties', *Journal of the American Chemical Society*, 130(18), pp. 5883–5885. Available at: https://doi.org/10.1021/ja801173r.

5.3.   List of abbreviations

- GHG   Green House Gases
- IPCP   Intergovernmental Panel on Climate Change
- HER   Hydrogen Evolution Reaction
- Ppm   parts per million
- AuNCs   Gold NanoClusters
- AuNP   Gold NanoParticles
- GNR   Graphene Nanoribbons
- WE   Working Electrode
- RE   Reference Electrode
- CE   Counter Electrode
- CB   Carbon Black
- G   Graphene
- GN   N-doped Graphene
- GS   S-doped Graphene
- AuG   Gold Clusters on Graphene
- AuGN   Gold Clusters on N-doped Graphene
- AuGS   Gold Clusters on S-doped Graphene
- AuCB   Gold Clusters on Carbon Black
- CP   Carbon Paper
- WE   Working Electrode
- CV   Cyclic Voltammetry
- XPS   X-Ray Photoelectron Spectroscopy
- TEM   Transmission electron microscopy
- STEM   Scanning transmission electron microscopy
- GC   Gas Chromatograph
- NMR   Nuclear Magnetic Resonance
- CV   Cyclic Voltammetry
- CA   Chronoamperometry
- FE   Faradaic Efficiency
- RHE   Reversible Hydrogen Electrode
- BE   Binding Energy